



# Influence of water content on the basic friction angle of porous limestones—experimental study using an automated tilting table

Á. Rabat<sup>1</sup> · R. Tomás<sup>1</sup> · M. Cano<sup>1</sup> · I. Pérez-Rey<sup>2</sup> · J. S. Siles<sup>1</sup> · L. R. Alejano<sup>3</sup>

Received: 25 December 2021 / Accepted: 1 April 2022 / Published online: 5 May 2022  
© The Author(s) 2022

## Abstract

An accurate evaluation of the shear strength of discontinuities is frequently a key aspect for determining the safety of mining and civil engineering works and for solving instability issues at rock mass scale. This is usually done by using empirical shear strength criteria in which the basic friction angle ( $\varphi_b$ ) is a relevant input parameter. Tilt testing is probably the most widespread method to obtain the  $\varphi_b$  due to its simplicity and low cost, but previous research has demonstrated that the results are strongly affected by several factors (e.g. surface finishing, cutting speed, specimen geometry, wear, time and rock type). In this connection, despite it is well known that water significantly reduces the mechanical properties of sedimentary rocks, very scarce research has focused on assessing the impact of the variations in water content on tilt test results. With the aim to fill this gap, saw-cut slabs of three limestone lithotypes were tilt tested in dry state, wet condition (fully water saturated, non-submerged samples) and under exposure to an environmental relative humidity (RH) of 90%. The results revealed that full water saturation caused moderate  $\varphi_b$  reductions in two lithotypes and a  $\varphi_b$  increase in one lithotype. This can be explained by their different microstructure and mineralogy, which makes that lubrication effect prevails over suction effect or vice versa. However, the exposure to a high RH environment did not cause significant  $\varphi_b$  variations. In addition, some important considerations related to tilt testing are provided and discussed, such as the intrinsic variability of the sliding angle ( $\beta$ ) and the impact of multiple sliding on the same rock surfaces on  $\beta$ .

**Keywords** Basic friction angle · Porous limestones · Tilt test · Relative humidity · Water saturation

## Symbols and abbreviations

$\underline{\beta}$	Sliding angle	$\varphi$	Internal friction angle
$\bar{\beta}$	Mean of the sliding angle values	$\varphi_b$	Basic friction angle
$\mu$	Coefficient of friction	$\overline{\varphi_b}$	Mean of the basic friction angle values
$\rho_b$	Bulk density	$\overline{\varphi_{bdry}}$	Mean of the basic friction angle values of dry specimens
$\tau$	Peak shear strength of the discontinuity	$\overline{\varphi_{bsat}}$	Mean of the basic friction angle values of fully water-saturated specimens
$\sigma_n$	Normal stress to which discontinuity is subjected	$\overline{\varphi_{bRH=90\%}}$	Mean of the basic friction angle values of specimens exposed to a RH = 90%
$\sigma_\beta$	Standard deviation of the sliding angle values	$\varphi_r$	Residual friction angle
$\sigma_{\varphi_b}$	Standard deviation of the basic friction angle values	$c_p$	Peak cohesion
		$c_a$	Apparent cohesion of the Patton's criterion
		$d_M$	Mean pore diameter
		EDX	Energy dispersive X-ray spectroscopy
		$E_{st}$	Static Young's modulus
		$h$	Height of the rectangular rock slab
		$I_{s(50)}$	Point load strength index
		$i$	Angle of the saw-tooth face of the Patton's criterion
		JCS	Joint-wall compressive strength
		JRC	Joint roughness coefficient

✉ Á. Rabat  
alvaro.rabat@ua.es

<sup>1</sup> Department of Civil Engineering, Escuela Politécnica Superior de Alicante, University of Alicante, P.O. Box 99, E-03080 Alicante, Spain

<sup>2</sup> Geotechnical Laboratory, CEDEX, Madrid, Spain

<sup>3</sup> Department of Natural Resources and Environmental Engineering, GESSMin Group, CINTECX, University of Vigo, Vigo, Spain

$K_{hd}$	Ratio between $\tan(\overline{\varphi_{bRH=90\%}})$ and $\tan(\overline{\varphi_{bdry}})$
$K_{sd}$	Ratio between $\tan(\overline{\varphi_{bsat}})$ and $\tan(\overline{\varphi_{bdry}})$
$l$	Length of the rectangular rock slab
MIP	Mercury intrusion porosimetry
$M_z$	Mean grain size
PLM	Polarised light microscopy
$p$	Total porosity
$p_o$	Open porosity
$R$	Schmidt hammer rebound number for dry non-weathered saw-cut rock surfaces
$r$	Schmidt hammer rebound number for weathered and wet discontinuity rock surfaces
RH	Relative humidity
SEM	Scanning electron microscopy
$T$	Temperature
UCS	Uniaxial compressive strength
$v_p$	P-wave velocity
$v_s$	S-wave velocity
$w$	Width of the rectangular rock slab
$w_c$	Water content
$w_e$	Equilibrium water content associated with a RH = 90%
XRD	X-ray diffraction

## Introduction

Rock masses typically consist of a rock matrix intersected by discontinuities such as shear zones, faults, joints, schistosity, bedding planes or flaws. This discontinuous nature of rock masses implies that their mechanical behaviour can sometimes be controlled by the presence and characteristics of discontinuities rather than by the intact rock (Ghazvinian et al. 2012). Considering this fact is especially relevant from a safety perspective in the execution and the design of civil engineering works and mining activities performed on shallow rock masses subjected to low confining pressures where instability phenomena are usually related to sliding or separation occurrences of rock blocks (e.g. rocky slopes, tunnels, open-pits, near-surface and underground excavations or rock-socketed piles) (Wines and Lilly 2003; Alejano et al. 2008, 2010, 2011, 2012b). Therefore, an accurate determination of the shear strength of discontinuities is of paramount importance for assessing and solving structurally controlled stability issues at rock mass scale (Kveldsvik et al. 2008; Ulusay and Karakul 2016; Pérez-Rey et al. 2019b).

Shear strength of discontinuities can be determined through in situ and laboratory investigation by carrying out direct shear tests or can be empirically estimated by using existing shear strength criteria (Hencher and Richards 2015). Because direct shear tests require an expensive shear test apparatus and involve difficult and time-consuming

procedure of specimen preparation and data processing, many empirical shear strength criteria have been developed so far and their use have been widely expanded among rock engineering practitioners (Singh and Basu 2018).

The vast majority of these criteria are based on Coulomb's linear formulation (1766); i.e. they relate the shear strength component, through normal stress, with different mechanical and surface-topography parameters of the joints. In particular, Patton's bilinear model (1966), given by Eqs. (1) and (2), can be considered as the first attempt to describe the peak shear strength of discontinuities with asperities (saw-tooth shape joints). Originally, Patton proposed to consider first order asperities to evaluate shear strength (Wyllie and Mah 2004).

However, later, Barton (1973) stated that for low normal stress ( $\sigma_n$ ), the second order roughness come into play:

$$\tau = \sigma_n \cdot \tan[\varphi_b + i] \quad (1)$$

In contrast, for high  $\sigma_n$  values, the asperities are sheared off with the displacement:

$$\tau = c_a + \sigma_n \cdot \tan[\varphi_r] \quad (2)$$

where  $\tau$  is the peak shear strength of the discontinuity,  $\sigma_n$  is the normal stress at which the discontinuity is subjected,  $\varphi_b$  is the basic friction angle,  $i$  is the angle of the saw-tooth face,  $c_a$  is the apparent cohesion and  $\varphi_r$  is the residual friction angle.

Subsequently, Barton and Choubey (1977) proposed an enhanced model applicable to rock joints with irregular surfaces (3), which has become one of the most widespread shear strength criteria, probably because of its simplicity, reliability on obtaining the input parameters and certain conservativeness (Pérez-Rey 2019).

$$\tau = \sigma_n + \tan\left[\varphi_r + JRC \cdot \log_{10}\left(\frac{JCS}{\sigma_n}\right)\right] \quad (3)$$

where JRC is the joint roughness coefficient, JCS is the joint-wall compressive strength and  $\varphi_r$  is the residual friction angle given by Eq. 4.

$$\varphi_r = (\varphi_b - 20) + 20 \cdot \left(\frac{r}{R}\right) \quad (4)$$

where  $r$  and  $R$  are the Schmidt hammer rebound number for weathered and wet discontinuity surfaces and for dry non-weathered saw-cut surfaces of the same rock, respectively.

As is clear from Eqs. 1, 3 and 4,  $\varphi_b$  is a crucial input parameter for the determination of the shear strength of discontinuities. It symbolises the shear strength between two planar (non-dilating), unfilled, non-weathered and non-polished rock surfaces (Pérez-Rey 2019). This property can be obtained by means of different laboratory tests such as

direct shear, push/pull and tilt tests. Nevertheless, among them, tilt test has been possibly the most widely used in rock engineering projects due to its greater simplicity, speed and low cost (Zhang et al. 2018).

Tilt test consists of placing rock specimens one on top to another in such a way that the surface of the plane of contact, which is initially horizontal, is progressively tilted until the upper specimen slides along the joint. The tilting angle with respect to the horizontal just at the instant when displacement begin is the  $\varphi_b$ . Different procedures have been historically used with regard the type of contact provided by the geometry of the samples: on the one hand, the three-core method (Stimpson 1981; Li et al. 2019), and the two-core method (Barton 2011; Ruiz and Li 2014) in which the contacts are linear; and on the other hand, the one-core method (Barton 1973; Zhang et al. 2018) and the block-based method (Alejano et al. 2012a; Ulusay and Karakul 2016) in which the contacts are planar surfaces. However, among them, the block-based method has proved to be the most suitable (specially, when slab-like specimens are used) because of core-based methods overestimate or do not provide reliable  $\varphi_b$  values (Alejano et al. 2012a; González et al. 2014). Furthermore, a great experimental effort has been done in previous works to detect other factors that influence tilt test results, such as the saw blades and cutting velocities (Alejano et al. 2017), the specimen size and shape (Hencher 1977; Alejano et al. 2012a; Kim et al. 2016; Jang et al. 2018), the test platform tilting rate and vibrations (Hencher 1977; Pérez-Rey et al. 2016, 2019a; Jang et al. 2018), the wear of rock surfaces due to multiple sliding on the same contact (Pérez-Rey et al. 2015, 2016, 2019a) or the time elapsing between cutting and testing (Pérez-Rey et al. 2015); as well as to evaluate the repeatability of tests carried out in different laboratories (Alejano et al. 2017). As a result of the conclusions derived from the abovementioned studies, an ISRM Suggested Method for determining the  $\varphi_b$  of planar rock surfaces using tilt tests has been recently published (Alejano et al. 2018). This document briefly points out that, although it is not fully recognised, other additional aspects such as environmental relative humidity (RH) or water content ( $w_c$ ) of specimens may affect the results of tilt tests in some friable rocks due to water and could activate adhesion between slickensided rock surfaces (Mehrishal et al. 2016).

Contact mechanic approaches have also been widely applied for studying rock interfaces. Misra and Marangos (2011) used a micromechanical model that explicitly considers asperity interactions on joint surfaces to examine the rock-joint closure and wave propagation behaviour. They concluded that rock joints with the same roughness can display a variety of closure behaviours depending on initial overlap of the joints and rock intrinsic friction. Recently, Kasyap and Senetakis (2021) utilised micromechanical-based experiments to analyse the effect of shearing rate on

the tangential contact behaviour of smooth flat quartz surfaces in the presence of plastic and non-plastic gouges. Their results indicated that important variations in the stick–slip instability (increase in force-drop, recurrence interval and slip velocity) occurred when the shearing rate was reduced by one order of magnitude. They also reported that the initial tangential stiffness raised when the shearing rate was diminished.

Conventional direct shear tests have frequently shown that moisture caused important reductions of the peak shear strength and friction angle ( $\varphi$ ) of unfilled discontinuities of sedimentary weak rocks, such as marls (Pellet et al. 2013) or claystones (Zandarin et al. 2013). In this line, micromechanical experiments performed to understand the tribological behaviour of analog mudrock interfaces have also indicated that the presence of water at the interfaces of these materials resulted in a continuous decrease of the friction compared to the dry state due to a predominant effect of abrasion (Ren et al. 2022). Also, substantial water-induced decreases of the frictional strength have been found in unfilled joints of other rock types, such as granitic gneiss (Jaeger 1959), trachyte (Hoskins et al. 1968), chalks (Gutierrez et al. 2000) or coal measure rocks (Li et al. 2005). In the case of filled joints, there might be development of suction which may provide additional contributing mechanics of friction. In this connection, Kasyap and Senetakis (2020) conducted micromechanical shearing tests which demonstrated that the presence of gouge materials between nominally flat quartz grains resulted in a reduction of frictional strength in comparison with pure quartz surfaces. Furthermore, they observed that plastic gouge materials (montmorillonite) exhibited a significant reduction in friction coefficient ( $\mu$ ) due to water submersion at any state of the shearing while non-plastic gouge materials (silt) showed only a slight decrease in the  $\mu$ .

Regarding the variations of the  $\varphi_b$  with moisture for saw-cut rock surfaces, inconsistent findings (reductions and increases) have been informed in literature. On the one hand, Barton (1973, 1977) collected the  $\varphi_b$  values of different rock types from earlier researchers (Patton (1966), Coulson (1972) and Richards (1975)) and concluded that dry specimens generally exhibited higher  $\varphi_b$  values than the wet ones. Subsequently, similar findings were also obtained by Aydan (1995), who attributed the results to the uncertainty of the effective normal stress over the shearing section. On the other hand, Ulusay and Karakul (2016) determined the  $\varphi_b$  values of 22 rock types from Turkey under dry, wet and submerged conditions using rectangular-based slabs. They found that in 13 rock types, wet  $\varphi_b$  was lower than dry  $\varphi_b$  (decreases between 1.4 and 10.6°) due to the predominance of the lubrication effect, while in the other 9 rock types, the wet  $\varphi_b$  was greater than the dry  $\varphi_b$  (increases between 0.2 and 6.5°) due to prevalence of the capillary action (suction). Furthermore, they reported that all dry samples displayed

higher  $\varphi_b$  values than submerged ones and that the reductions of  $\varphi_b$  widely varied between 0.2 and 15.2° because the lubrication effect happened with different intensity according to the mineral composition of each rock type. In the same vein, Zhang et al. (2018) obtained the  $\varphi_b$  values of 46 rock types from Norway in dry and wet states using cylindrical specimens (three-core method). They reported that 21 rock types exhibited wet  $\varphi_b$  values smaller than the dry ones (with drops between 0.7 and 5.3°) while the remaining 25 rock types showed the opposite behaviour (with increments between 0.7 and 5.0°). These authors postulated that the impact of humidity on  $\varphi_b$  was not linked to lithology but rather to mineralogy. Later, Kim and Jeon (2019) evaluated

the water-induced changes in  $\varphi_b$  on granite, diorite, sandstone and cement mortar and found increases ranging from 1 to 3°. Recently, Beyhan and Özdemir (2021) measured the  $\varphi_b$  of travertine's samples under dry and different soaked conditions (i.e. water solutions with a pH of 2, 7 and 12) and observed that those conditioned at pH of 2 displayed the lowest values while those conditioned under the rest of conditions exhibited quite similar values between them. A summary of the  $\varphi_b$  values in dry and wet conditions found in preceding works for different rock types is given in Table 1.

Petrological characteristics and microstructure of geo-materials are also additional factors that affect frictional properties of rock surfaces and their water-induced changes.

**Table 1** Basic friction angle ( $\varphi_b$ ) values in dry and wet conditions found in literature for different rock types

Authors	Basic friction angle $\varphi_b$ (°)		Rock type
	Dry	Wet	
Patton (1966)	26–35	25–33	Sandstone
Barton (1971)	31	31	Porphyry
Coulson (1972)	31–37	27–35	Dolomite
	37–40	35–38	Limestone
	31–33	27–31	Siltstone
	32–34	31–34	Sandstone
	35–38	31–36	Basalt
	31–35	29–31	Fine-grained granite
	31–35	31–33	Coarse-grained granite
	26–29	23–26	Gneiss
	Richards (1975)	36	32
30		21	Slate
Ulusay and Karakul (2016)	27.9–32.0	28.3–30.4	Andesites
	28.2–38.3	29.7–36.6	Travertines
	30.8–36.7	26.1–35.3	Ignimbrites
	30.9	31.1	Basalt
	22.5	29.0	Granite
	32.3	30.3	Carbonated serpentinite
	25.9–37.6	26.7–34.8	Limestones
	36.7	32.6	Marble
	Zhang et al. (2018)	30.2	31.7
30.1		29.4	Quartz sandstone
28.0–36.1		31.6–33.1	Granites
28.8		31.1	Gabbro
25.1–28.7		28.9–29.8	Monzonites
33.2		30.8	Pegmatite
32.1		30.0	Migmatite
32.0–34.5		30.7–33.4	Amphibolite
Kim and Jeon (2019)		30	31
	29	32	Diorite
	28	31	Sandstone
	34	36	Cement mortar
Beyhan and Özdemir (2021)	31.6	25.6 (pH of 2)	Travertines
		32.1 (pH of 7)	
		30.4 (pH of 12)	



Cruden and Hu (1988) found that the  $\phi_b$  of carbonate rocks depends on grain size and mineralogy. In particular, they obtained that for pure carbonate rocks, the  $\phi_b$  reduces with increasing dolomite content and decreasing grain size. Ramana and Gogte (1989) reported that rocks rich in felsic minerals, quartz and calcite exhibit higher  $\mu$  values than rocks with significant hydroxyl bearing minerals. Horn and Deere (1962) indicated that as surface moisture rises, the  $\mu$  of massive-structured minerals (e.g. quartz, feldspar and calcite) increases. In contrast, they observed that the  $\mu$  reduces when surface moisture increases for layer lattice minerals (e.g. muscovite, phlogopite, biotite, chlorite, serpentine, steatite and talc). Also, Morrow et al. (2000) reported that moisture caused no substantial or slight  $\mu$  modifications for calcite, quartz, albite and zeolites (i.e. laumontite and clinoptilolite), dramatic drops for serpentinites (i.e. antigorite, lizardite and chrysotile) and moderate decreases for sheet-structures minerals (i.e. kaolinite, muscovite, chlorite, brucite and talc). Tembe et al. (2010) observed that the  $\mu$  of saturated binary and ternary mixtures made up of quartz, montmorillonite and illite decreased with increasing clay content. Furthermore, Westbrook et al. (1968) and MacMillan et al. (1974) have demonstrated that the adsorption of fluids in mineral surfaces could cause significant variations in their surface microhardness.

The abovementioned background has shown that (1) there is a lack of studies regarding the effect of the environmental relative humidity and moisture content of samples on tilt test results; (2) inconsistent findings have been obtained concerning the water-induced changes in the  $\phi_b$  of rocks; and (3) the underlying causes of this behaviour are unclear and may be related to petrophysical properties of rocks. This research addresses and tries to elucidate these points for carbonate rocks. To this aim, a tilt testing campaign was carried out in three limestone lithotypes (calcarenites). In particular,  $\phi_b$  values were measured in saw-cut rock-like slab specimens tested under three different conditions: (1) oven-dry state, (2) non-submerged but fully water-saturated state achieved by using vacuum and (3) partially water-saturated state reached by equilibrating the rock samples with an environment of high relative humidity (90%). Complementarily, mineralogy and microstructural characteristics (grain and pore sizes) of these rocks are analysed with the aim of linking the  $\phi_b$  values and their water-induced variations with them.

## Materials and methods

### Tested rocks and specimen preparation

Tested carbonate rocks are three porous limestone lithotypes (calcarenites) commercially known as *Blue*, *Beige* and *Diamond Bateig* stones (hereinafter labelled as S-1, S-2 and S-3,

respectively) that were extracted from an active quarry located in the municipality of Elda (Alicante, south-eastern Spain). They belong to a Tertiary transgressive unit (Middle-Upper Miocene) (Ordoñez et al. 1994). These rocks are composed of primary sediments corresponding to the continental shelf and a discontinuous deposition characterised by an abundant presence of planktonic, nektonic and benthic organisms. Specifically, detrital and diagenetic silicates and organic fossils (principally foraminifera) are their main constituents (Ordóñez et al. 1997; Fort et al. 2010).

Recent research has shown that the rock matrix of these limestone varieties exhibits important physico-mechanical changes when they become completely water-saturated (Rabat et al. 2020a, c) or when they are subjected to high environmental relative humidities (Rabat et al. 2020b), as well as that pore water distribution plays a key role in this water-induced mechanical weakening (Rabat et al. 2021). However, to date, there are no scientific works examining the water-induced variations in  $\phi_b$  of saw-cut surfaces of these rocks, which has motivated the present article. The results of a general physico-mechanical characterisation of the rock matrix of these calcarenites are shown in Table 2.

Rock specimens of each calcarenite variety intended for tilt testing were obtained from a  $60 \times 20 \times 7.5$  cm<sup>3</sup> prismatic unweathered rock block that was cautiously selected to guarantee its homogeneity and the absence of visible fractures. All rock blocks were cut into slabs using the same circular saw-blade (600 mm in diameter and 3.5 mm in thickness) and cutting velocity regardless of their subsequent water treatment. In addition, special care was taken to avoid undesirable contacts between the pristine slab surfaces and other objects that could damage the specimens.

In particular, a total of 36 rectangular-based specimens (12 units of each lithotype) with dimensions of about  $10.0 \times 7.5 \times 1.5$  cm<sup>3</sup> (length,  $l \times$  width,  $w \times$  height,  $h$ ) were prepared in order to fulfil the geometrical recommendations

**Table 2** Physical and mechanical properties of the rock matrix of the tested calcarenites in dry condition (Rabat et al. 2020a, c, 2021)

Physical or mechanical property	Limestone lithotypes		
	S-1	S-2	S-3
Open porosity, $p_o$ (%)	11.7	18.1	20.3
Total porosity, $p$ (%)	14.9	20.3	21.7
Bulk density, $\rho_b$ (kg/m <sup>3</sup> )	2292	2165	2122
P-wave velocity, $v_p$ (m/s)	4613	3318	4174
S-wave velocity, $v_s$ (m/s)	2656	2030	2408
Uniaxial compressive strength, UCS (MPa)	36.6	21.5	26.9
Static Young's modulus, $E_{st}$ (GPa)	25.0	7.7	19.9
Point load strength Index, $I_{s(50)}$ (MPa)	3.9	1.8	2.8
Peak cohesion, $c_p$ (MPa)	21.6	12.5	16.9
Internal friction angle, $\phi$ (°)	37.4	35.3	27.3

specified in the ISRM Suggested Method (Alejano et al. 2018), that are,  $l/h > 6$  (in our case, it was 6.67),  $w/h > 4$  (in our case, it was 5.00) and  $l \times w > 50 \text{ cm}^2$  (in our case, it was  $75.00 \text{ cm}^2$ ) (Fig. 1). Once the rock slabs were cut, they were washed with distilled water to remove excess dust particles from the contact surfaces. Afterwards, they were dried in an oven at a temperature (T) of  $70 \text{ }^\circ\text{C}$  during 48 h. Finally, they were preserved in laboratory conditions (T =  $20 \text{ }^\circ\text{C}$  and RH = 50%) until they were subjected to the corresponding treatment prior to tilt testing.

Given that 12 rectangular-based specimens (labelled from 1 to 12) were obtained for each calcarenite variety and that each specimen had two surfaces (labelled as *a* and *b*), 12 contacts of each lithotype were available for tilt testing (i.e. 1b–2a, 1a–2b, 3b–4a, 3a–4b, 5b–6a, 5a–6b, 7b–8a, 7a–8b,

9b–10a, 9a–10b, 11b–12a and 11a–12b). Specimens (or contacts) of each calcarenite were divided into three groups (4 units or contacts per group) that were subjected to different treatments (Fig. 1).

The first group (i.e. 1b–2a, 1a–2b, 3b–4a and 3a–4b) was dried in a ventilated oven at  $105 \text{ }^\circ\text{C}$  until a constant mass of specimens was obtained. Then, they were kept in a desiccator until they reached the ambient temperature. Finally, tilt tests were carried out using these dry specimens under laboratory conditions (T =  $20 \text{ }^\circ\text{C}$  and RH = 50%).

The second group (5b–6a, 5a–6b, 7b–8a and 7a–8b) was soaked in distilled water inside a vacuum chamber during 48 h, which is a period of time longer than what is required to fully water-saturate these rock materials. The water contents ( $w_c$ ) associated with this testing condition were

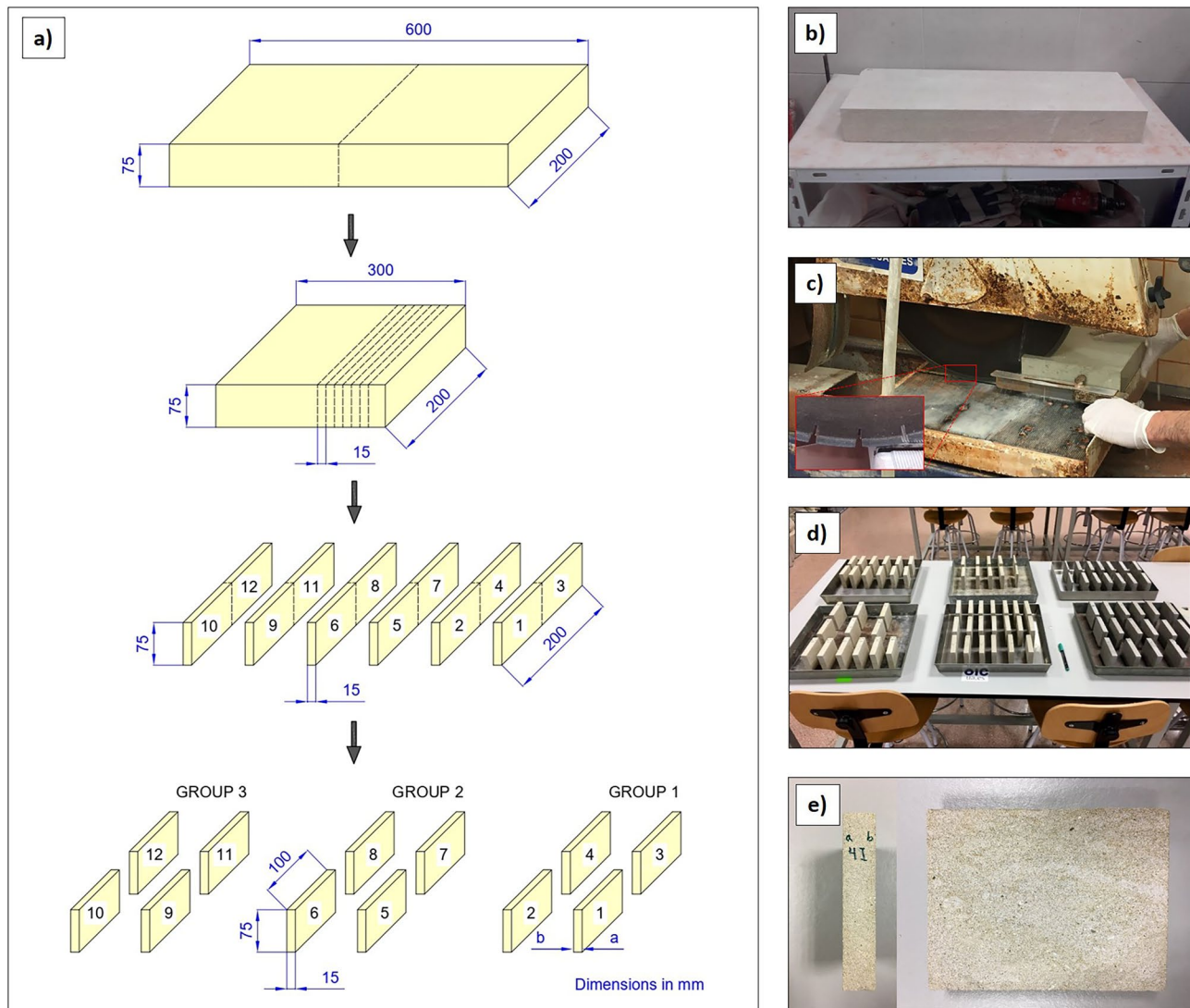


**Fig. 1** (a) Scheme of the cutting process to obtain the calcarenite slabs used in tilt tests. (b) Original rock block ( $60 \times 20 \times 7.5 \text{ cm}^3$ ). (c) Cutting machine and detail of the saw blade disc. (d) Overview of rock samples. (e) Detail of a calcarenite slab specimen ( $10.0 \times 7.5 \times 1.5 \text{ cm}^3$ )

$4.93 \pm 0.42\%$  in calcarenite S-1,  $8.67 \pm 0.51\%$  in calcarenite S-2 and  $9.23 \pm 2.10\%$  in calcarenite S-3. Finally, tilt tests were performed on these water-saturated specimens at laboratory conditions ( $T = 20\text{ }^{\circ}\text{C}$  and  $\text{RH} = 50\%$ ).

The third group (9b–10a, 9a–10b, 11b–12a and 11a–12b) was placed inside a controlled humidity chamber at constantly fixed conditions ( $T = 20\text{ }^{\circ}\text{C}$  and  $\text{RH} = 90\%$ ) during 10 days in order to reach the corresponding equilibrium water content ( $w_e$ ) inside pore network of these rocks. This high RH number was chosen because it could often correspond to the maximum RH value recorded in real environmental conditions. The average  $w_e$  values reached by the three lithotypes after the environmental relative humidity equilibrium were  $0.94 \pm 0.01\%$  in S-1,  $1.08 \pm 0.02\%$  in S-2 and  $0.62 \pm 0.01\%$  in S-3. Finally, tilt tests were carried out on these partially water-saturated specimens under the aforementioned environmental conditions ( $T = 20\text{ }^{\circ}\text{C}$  and  $\text{RH} = 90\%$ ).

### Mineralogical and microstructural characterisation

Mineralogical composition and microstructural properties of rocks were determined using X-ray diffraction (XRD) technique, polarised light microscopy (PLM), scanning electron microscopy (SEM) and mercury intrusion porosimetry (MIP). XRD analysis was carried out on rock powder using a Bruker D8-Advance XR diffractometer with a generator of

XR Kristalloflex K 760–80 F and a XR tube with a copper anode. PLM examination was conducted on thin-sections obtained in perpendicular direction of sedimentary bedding planes using an Optika B600POL petrographic microscope equipped with the  $\times 4$  objective lens. SEM analysis was performed on rock fragments of approximately  $1\text{ cm}^3$  using a Bruker Merlin VP compact apparatus with an accelerating voltage of 20 kV. In addition, energy dispersive X-ray spectroscopy (EDX) analysis was carried out using a Quantax 400 tool. MIP was conducted on rock fragments whose largest dimension was less than 9 mm using a Poremaster-60GT device equipped with two low and two high pressure stations up to 40,000 psi.

### Automated tilting table

Tilting table used in this research is a device designed by some of the co-authors of this article and protected through a utility model certificate (Tomás et al. 2021). Its main components are as follows: (a) a steel reinforced structure and a tilting platform that allow testing standardised rock specimens as well as large and heavy rock blocks and other geomaterials; (b) a power regulator that controls the speed of the lifting system accurately and that reduces unwanted vibrations and accelerations during the test; (c) a system fully adaptable to the test geometry and equipped with a photoelectric cell for the detection of movement and automatic stop when the specimens start to

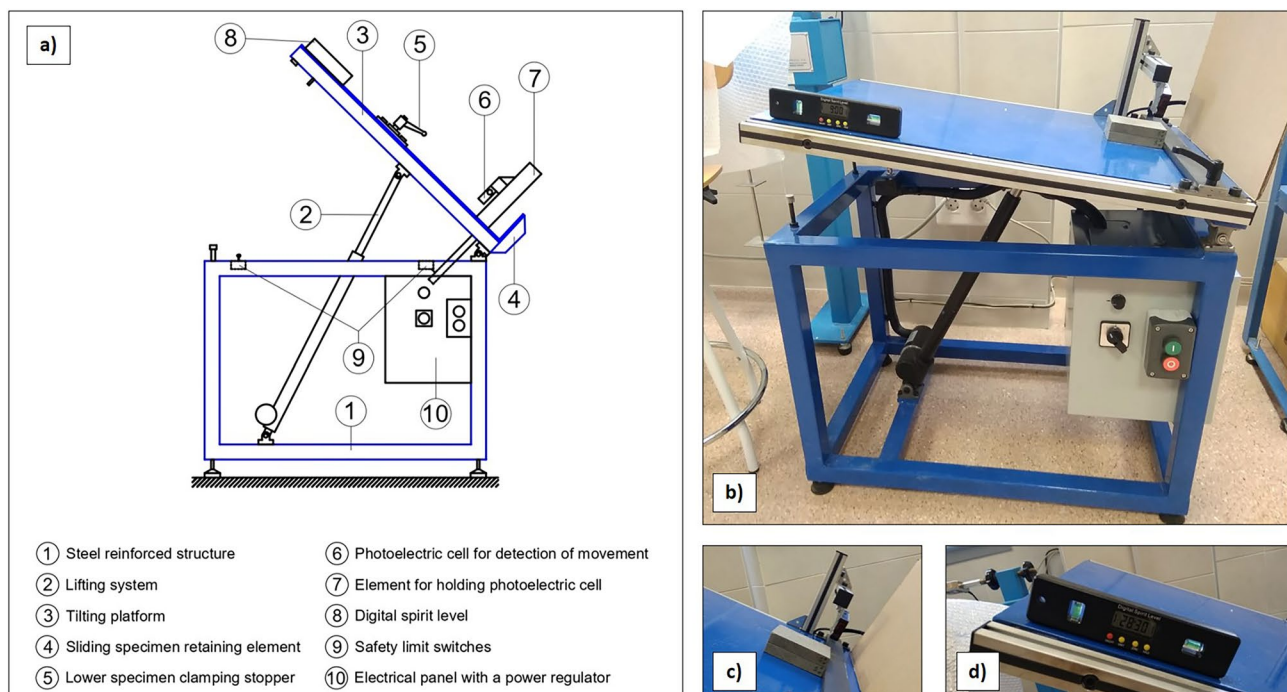


**Fig. 2** **a** Sketch of the automated tilting table showing its main components. **b** Tilt apparatus overview. **c** Detail of the photoelectric cell used for the automatic detection of the upper specimen movement. **d** Digital spirit level used to measure the sliding angle value



move; (d) a lower specimen clamping stopper that can be slid along the table to adjust it to the test requirements; (e) a digital spirit level that can measure the tilting angle with an accuracy of  $\pm 0.01^\circ$  (Fig. 2).

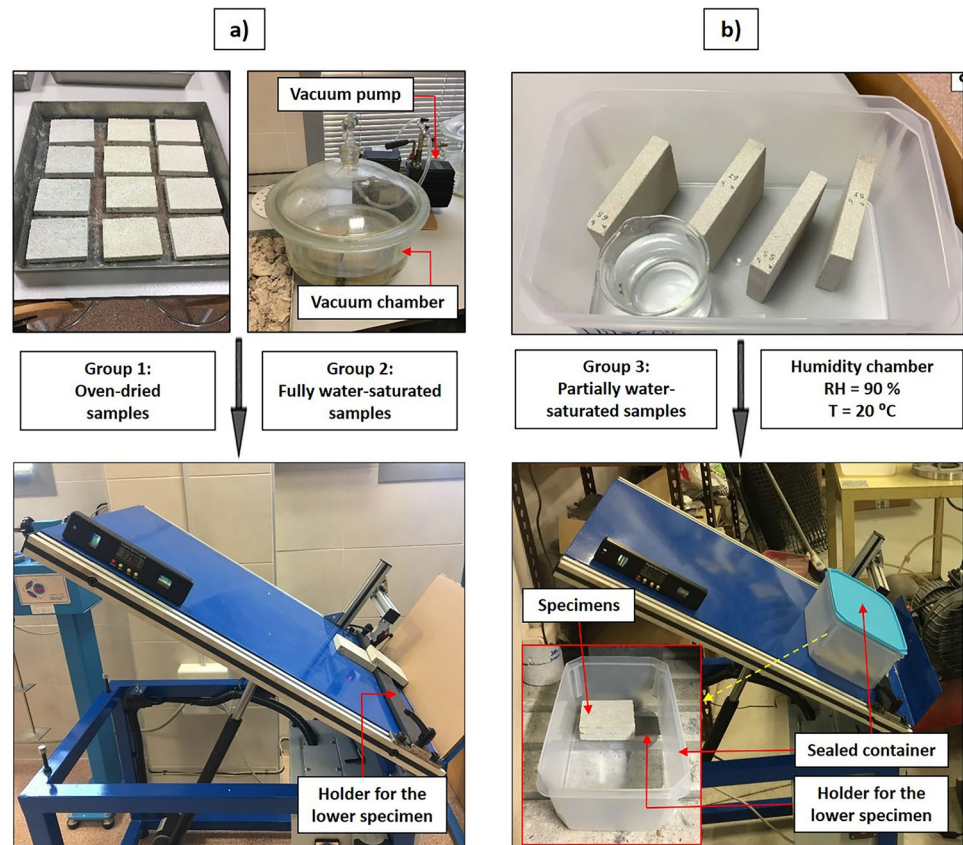
### Procedure for determining the basic friction angle

The procedure described below was used for determining  $\phi_b$ :

- (1) The lower rectangular slab for tests performed under dry and fully water-saturated conditions was fixed to the plane-tilting platform using a specimen holder and the upper slab was put on top of it. They were positioned in such a way that the sliding direction matched with the maximum dimension of the specimens (Fig. 3a). In the case of the tests carried out under a controlled RH of 90%, the specimens were tested inside a sealed container with this environmental RH (Fig. 3b).
- (2) The table was gradually tilted at a constant rotational-velocity of  $10^\circ/\text{min}$  until the initiation of sliding, which was defined as the instant at which the upper rock slab began to slide over the lower one. In the case of the tests performed on dry and fully water-saturated specimens, the beginning of the movement was automati-
- (3) cally detected by the photoelectric cell coupled to the tilting table. By contrast, in the case of the tests carried out under a controlled RH of 90%, the initiation of sliding was detected visually given that the specimens were tested inside a transparent sealed container and the photoelectric cell was not able to detect the movement. Then, the quasi-static sliding angle value ( $\beta$ ) displayed by the digital spirit level was recorded.
- (4) The  $\phi_b$  of each pair of contact surfaces was calculated as the median value of the five repetitions performed.

$$\Phi_b = \text{median } \beta_{j=1,\dots,5} \quad (5)$$

**Fig. 3** Setups used for determining the basic friction angle ( $\phi_b$ ) in dry and fully water-saturated specimens (a) as well as in the specimens exposed to a controlled RH of 90% (b)



## Results and analysis

### Mineralogy and microscopic properties

S-1 is a sandy fossiliferous limestone (biocalcarene) with a mean grain size of 0.2 mm. PLM and SEM techniques revealed that this lithotype is mainly constituted of fossils (60%) with a size varying from 0.1 to 0.4 mm, such as foraminifera (e.g. Rotalidae, Globigerinidae, Textularidae and Globorotalia), echinoderms and bryozoans. Terrigenous components account for 15% and exhibit a crystal size fluctuating among 0.1 and 0.3 mm. They consist predominantly of monocrystalline and polycrystalline quartz, dolomite, phyllosilicates, potassium feldspar, tourmaline and muscovite. Its orthochemical components represent

15% and are micritic matrix (10%), sparry cement (5%) and a small fraction of siliceous fibrous cement (Fig. 4a.2, a.3, a.4). Accordingly, the semiquantitative mineralogical analysis determined by XRD technique showed that this rock variety is composed of calcite (86%), quartz (8%), dolomite (2%), phyllosilicates (2%) and other minority minerals (2%). MIP technique demonstrated that this lithotype mainly presents pores with diameters ranging from 0.1 to 1  $\mu\text{m}$  (53%) and from 0.01 to 0.1  $\mu\text{m}$  (25%), an interparticle porosity of 1%, an intraparticle porosity of 12% and a specific surface area of 5.5  $\text{m}^2/\text{g}$  (Fig. 5a, d).

S-2 is a sandy fossiliferous limestone (biocalcarene) with a mean grain size of 0.3 mm. PLM and SEM techniques showed that this variety is principally composed of fossils (55%) with a size ranging from 0.1 to 0.6 mm, such as

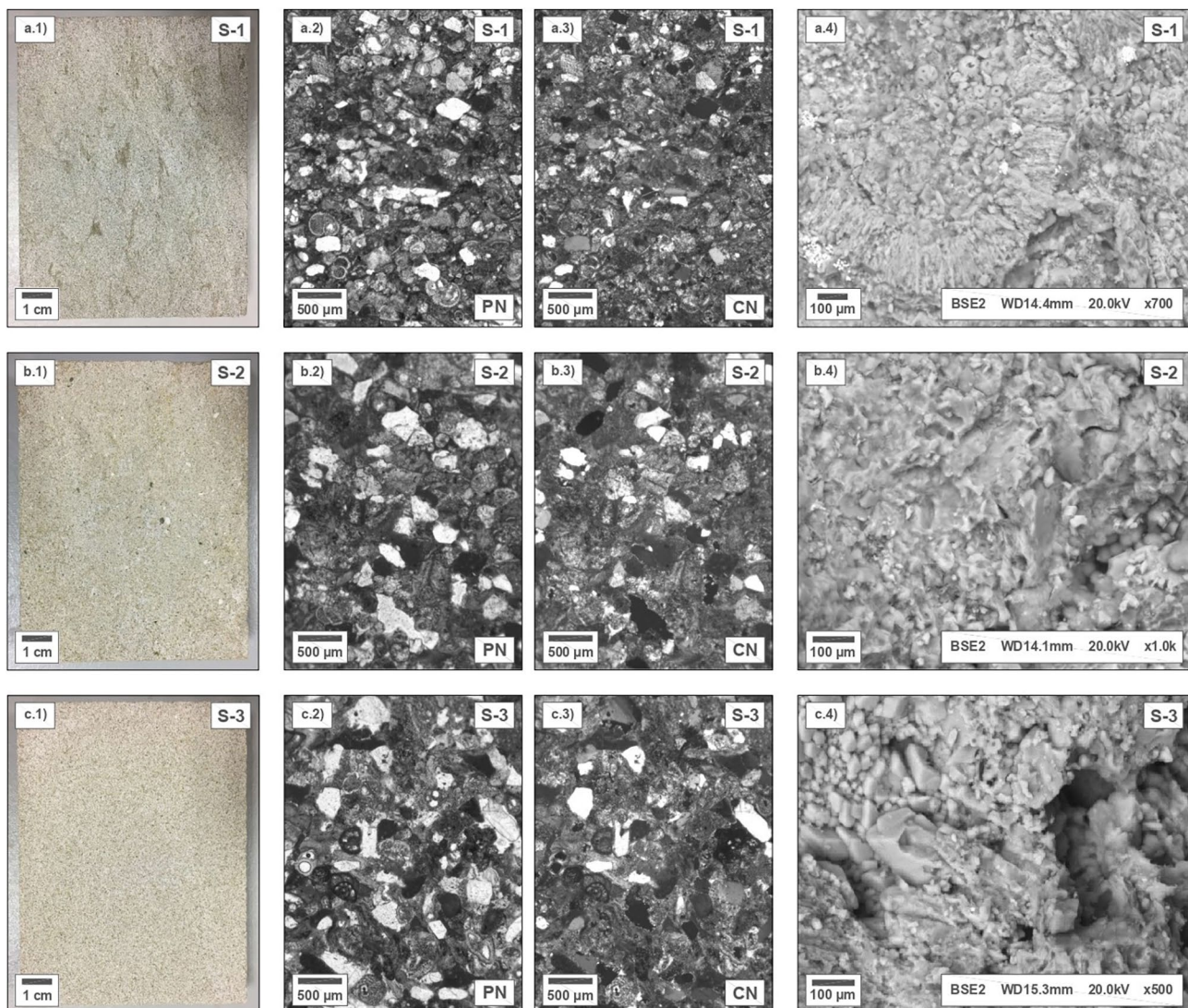


**Fig. 4** Surfaces of slab specimens before tilt testing (a.1, b.1 and c.1), thin-section microphotographs taken with parallel light (a.2, b.2 and c.2) and crossed nicols (a.3, b.3 and c.3) and SEM images (a.4, b.4 and c.4) of the tested rocks



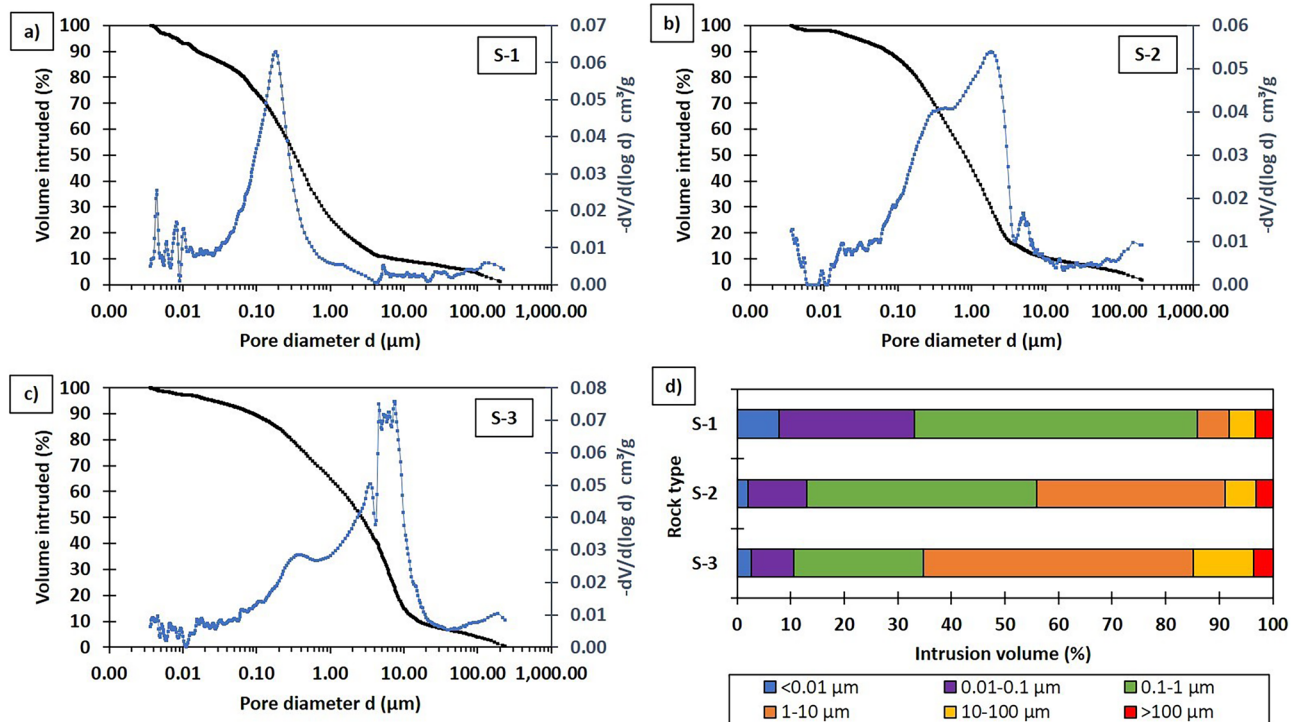


**Fig. 5** Cumulative mercury intrusion and pore-size distribution curves of S-1 (a), S-2 (b) and S-3 (c) and comparative analysis between calcarenites (d)

foraminifera (e.g. Globigerinidae, Textularidae and Rotalidae), molluscs and bryozoans. Terrigenous components represent 15% and show a crystal size varying between 0.1 and 0.3 mm. They are made up of monocrystalline quartz, dolomite, phyllosilicates, potassium feldspar and muscovite. Its ortochemical fraction (18%) corresponds to micritic matrix (14%) and sparitic cement (4%) showing equicrystalline mosaics of calcite spar (Fig. 4b.2, b.3, b.4). In line with this, the semiquantitative mineralogical analysis obtained using XRD technique displayed that this lithotype is formed by calcite (85%), quartz (7%), phyllosilicates (5%), dolomite (2%) and other marginal minerals (1%). MIP technique revealed that this variety mostly exhibits pores with diameters fluctuating from 0.1 to 1  $\mu\text{m}$  (43%) and from 1 to 10  $\mu\text{m}$  (35%), an interparticle porosity of 3%, an intraparticle porosity of 16% and a specific surface area of 3.2  $\text{m}^2/\text{g}$  (Fig. 5b, d).

S-3 is a sandy fossiliferous limestone (biocalcarenite) with a mean grain size of 0.4 mm. PLM and SEM examinations indicated that this variety is mostly composed of fossils (60%) with a size varying from 0.3 to 0.6 mm, such as different foraminifera (e.g. Rotalidae, Heterostegina, Turborotalia and Globigerinidae). Terrigenous components account for 10% and present a crystal size ranging from 0.2 to 0.5 mm. They consist principally of monocrystalline quartz, dolomite, phyllosilicates, schist, potassium feldspar

and clay galls. Its ortochemical constituents represent 15% and consist mainly of micrite (Fig. 4c.2, c.3, c.4). In this connection, the semiquantitative mineralogical analysis performed through XRD technique revealed that this rock type is composed of calcite (87%), quartz (5%), phyllosilicates (5%), dolomite (2%) and other minority minerals (1%). MIP results displayed that this variety essentially has pores with diameters ranging from 1 to 10  $\mu\text{m}$  (50%) and from 0.1 to 1  $\mu\text{m}$  (24%), an interparticle porosity of 8%, an intraparticle porosity of 12% and a specific surface area of 3.2  $\text{m}^2/\text{g}$  (Fig. 5c, d).

### Sliding angle values and its variability with repetition and water content

The five sliding angle values ( $\beta$ ) obtained in each of the four tested contacts for each rock type and water content, as well as their associated mean values ( $\bar{\beta}$ ) and standard deviations ( $\sigma_{\beta}$ ), can be seen in Table 3.

In dry state (RH = 50% and T = 20  $^{\circ}\text{C}$ ), calcarenite S-1 exhibited the smallest  $\beta$  values, with numbers varying between 26.7 and 37.8 $^{\circ}$ , an average value of 31.8 $^{\circ}$ , a median of 31.8 $^{\circ}$  and a standard deviation of 2.5 $^{\circ}$ . On the contrary, calcarenite S-2 showed the highest  $\beta$  values, with figures fluctuating between 31.3 and 41.7 $^{\circ}$ , an average value of 37.4 $^{\circ}$ , a median of 37.3 $^{\circ}$  and a standard deviation

**Table 3** Sliding angle values ( $\beta_j$ ) measured in each tested contact (k) and their associated mean values ( $\bar{\beta}$ ) and standard deviations ( $\sigma_\beta$ )

Rock type (condition)	Serial no.	Serial code (dataset)	$\beta_1$ (°)	$\beta_2$ (°)	$\beta_3$ (°)	$\beta_4$ (°)	$\beta_5$ (°)	$\bar{\beta}$ (°)	$\sigma_\beta$ (°)
S-1 (dry)	1	S-1.D.1b-2a	33.1	33.3	31.5	29.4	31.9	31.8	1.4
	2	S-1.D.1a-2b	34.2	28.3	34.3	37.8	34.6	33.8	3.1
	3	S-1.D.3b-4a	29.7	26.7	28.8	31.5	29.7	29.3	1.6
	4	S-1.D.3a-4b	33.9	31.3	31.2	32.0	32.7	32.2	1.0
S-2 (dry)	1	S-2.D.1b-2a	34.3	41.7	37.8	36.7	36.8	37.5	2.4
	2	S-2.D.1a-2b	34.9	35.2	39.2	31.3	33.8	34.9	2.6
	3	S-2.D.3b-4a	39.0	41.3	39.8	40.8	41.5	40.5	0.9
	4	S-2.D.3a-4b	38.5	36.9	35.8	33.7	39.2	36.8	2.0
S-3 (dry)	1	S-3.D.1b-2a	31.7	32.2	38.3	36.6	35.0	34.8	2.5
	2	S-3.D.1a-2b	39.1	35.0	34.8	37.7	37.6	36.8	1.7
	3	S-3.D.3b-4a	37.6	38.7	37.4	39.0	37.4	38.0	0.7
	4	S-3.D.3a-4b	38.6	38.7	37.2	38.4	35.0	37.6	1.4
S-1 (fully water-saturated)	1	S-1.S.5b-6a	37.0	46.7	34.8	33.8	37.1	37.9	4.6
	2	S-1.S.5a-6b	30.8	31.4	34.6	30.0	29.1	31.2	1.9
	3	S-1.S.7b-8a	36.7	38.9	40.2	35.8	36.1	37.5	1.7
	4	S-1.S.7a-8b	33.1	31.7	39.3	28.6	29.4	32.4	3.8
S-2 (fully water-saturated)	1	S-2.S.5b-6a	32.9	33.8	31.8	31.3	32.8	32.5	0.9
	2	S-2.S.5a-6b	30.6	27.2	25.0	32.4	26.1	28.3	2.8
	3	S-2.S.7b-8a	30.1	37.6	30.7	36.5	29.8	32.9	3.4
	4	S-2.S.7a-8b	31.4	29.8	28.7	32.8	31.7	30.9	1.5
S-3 (fully water-saturated)	1	S-3.S.5b-6a	32.8	35.1	29.7	32.2	29.7	31.9	2.0
	2	S-3.S.5a-6b	38.3	29.1	38.7	34.7	27.9	33.7	4.5
	3	S-3.S.7b-8a	36.7	21.5	30.2	33.8	33.2	31.1	5.2
	4	S-3.S.7a-8b	33.0	25.8	28.7	36.5	31.9	31.2	3.7
S-1 (RH=90%)	1	S-1.H.9b-10a	31.5	33.1	30.9	34.7	32.3	32.5	1.3
	2	S-1.H.9a-10b	33.9	38.3	35.5	33.1	38.9	35.9	2.3
	3	S-1.H.11b-12a	29.1	32.1	32.3	31.5	33.3	31.7	1.4
	4	S-1.H.11a-12b	31.6	31.2	29.9	29.8	33.8	31.3	1.5
S-2 (RH=90%)	1	S-2.H.9b-10a	37.2	40.3	40.0	33.2	36.4	37.4	2.6
	2	S-2.H.9a-10b	39.9	39.6	36.0	37.2	44.9	39.5	3.1
	3	S-2.H.11b-12a	37.5	35.6	36.3	37.1	39.9	37.3	1.5
	4	S-2.H.11a-12b	38.0	37.7	42.1	34.6	32.9	37.1	3.2
S-3 (RH=90%)	1	S-3.H.9b-10a	36.6	34.6	33.4	34.1	35.9	34.9	1.2
	2	S-3.H.9a-10b	37.5	35.1	36.8	38.6	36.2	36.8	1.2
	3	S-3.H.11b-12a	37.8	30.8	34.5	39.2	41.8	36.8	3.8
	4	S-3.H.11a-12b	34.4	32.3	35.8	36.3	30.6	33.9	2.1

of 2.9°. Calcarenite S-3 showed  $\beta$  values quite similar to those displayed by S-2, with numbers varying between 31.7 and 39.1°, an average value of 36.8°, a median of 37.5° and a standard deviation of 2.1°. Histograms, potential normal distributions associated with these mean values and standard deviations as well as the corresponding boxplots obtained from the twenty  $\beta$  determinations conducted on each rock type under dry condition can be seen in Fig. 6. Its analysis shows that data obtained in S-1 and S-2 fit reasonably well to a normal distribution (Fig. 6a, b), which is corroborated by a considerable symmetry of the boxplots in terms of ends and whiskers (Fig. 6d). However, the values measured in

calcarenite S-3 fit worse to a normal distribution (Fig. 6c) and the ends and whiskers of the boxplots are far from symmetrical. Furthermore, no outliers (values outside the whiskers) were obtained in any of the dry tested rocks.

In fully water-saturated state (RH = 50% and T = 20 °C), calcarenite S-1 displayed the greatest  $\beta$  values, with figures ranging from 28.6 to 46.7°, an average value of 34.8°, a median of 34.7° and a standard deviation of 4.4°. Calcarenites S-2 and S-3 exhibited close  $\beta$  values to each other. Specifically,  $\beta$  values were in the range of 25.0–37.6° in S-2 and of 21.5–38.7° in S-3, the average values were 31.2° in S-2 and 32.0° in S-3, the medians were 31.4° in S-2 and 32.5° in S-3

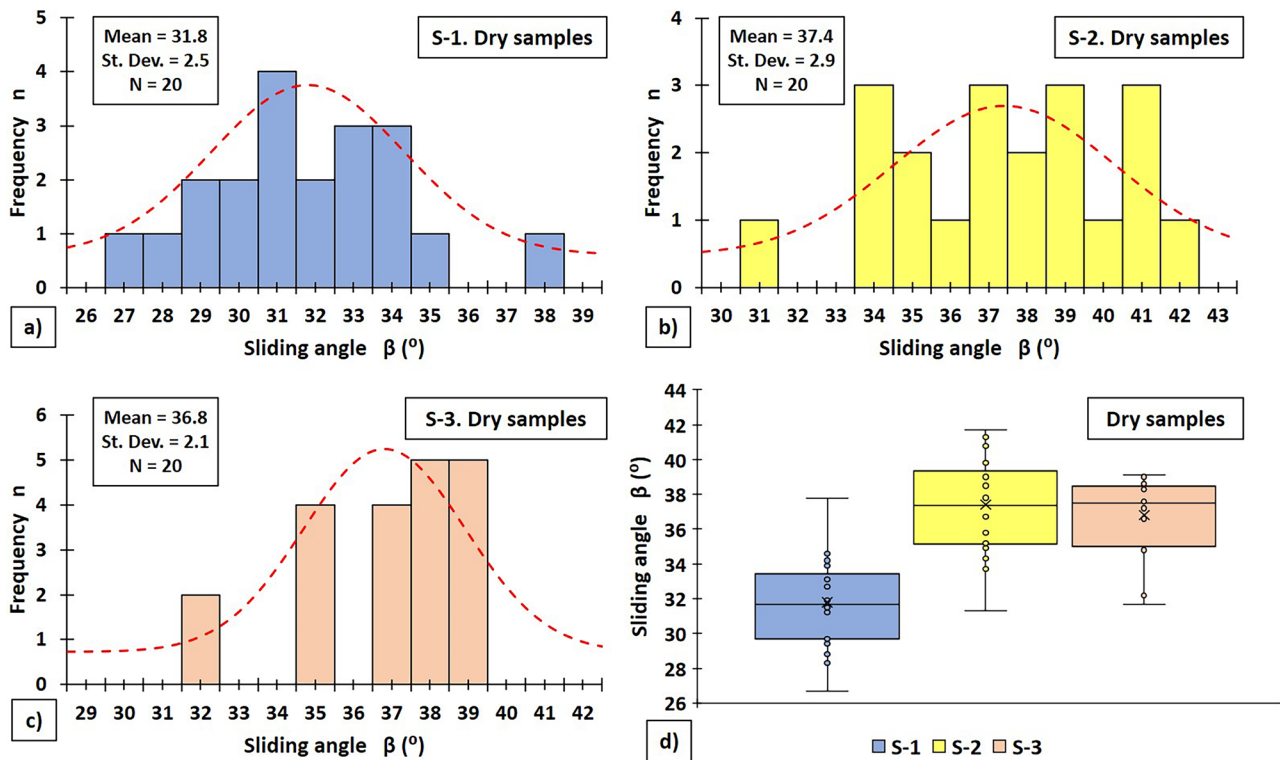


**Fig. 6** Histograms showing sliding angle values for five repetition of tilt tests conducted on four contact surfaces of S-1 (a), S-2 (b) and S-3 (c) under dry conditions and the corresponding box and whisker

plots comparing the results obtained in the three tested limestones. Dashed lines represent the fitted normal distribution

and the standard deviations were  $3.0^\circ$  in S-2 and  $4.2^\circ$  in S-3. In this case, histograms show that the  $\beta$  values obtained in the calcarenite S-1 fit worse to a normal distribution than the  $\beta$  values measured in the calcarenites S-2 and S-3 (Fig. 7a, b, c). Furthermore, the boxplots show the existence of outliers in the three fully water-saturated rocks (Fig. 7d) and a larger  $\beta$  variability compared to dry specimens.

Concerning the partially water-saturated samples by exposure to a high relative humidity environment (RH=90% and  $T=20^\circ\text{C}$ ), calcarenite S-1 showed the lowest  $\beta$  values, with figures ranging from  $29.1$  to  $38.9^\circ$ , an average value of  $32.8^\circ$ , a median of  $32.3^\circ$  and a standard deviation of  $2.5^\circ$ . In contrast, calcarenite S-2 exhibited the highest  $\beta$  values, with numbers varying between  $32.9$  and  $44.9^\circ$ , an average value of  $37.8^\circ$ , a median of  $37.4^\circ$  and a standard deviation of  $2.8^\circ$ . In calcarenite S-3 the  $\beta$  values fluctuated among  $30.6$  and  $41.8$ , the average value was  $35.6^\circ$ , the median was  $35.9^\circ$  and the standard deviation was  $2.7^\circ$ . Histograms indicate that the  $\beta$  values obtained in the three rocks fit quite well to a normal distribution (Fig. 8a, b, c) while the boxplots reveal that outliers were obtained in calcarenites S-1 and S-3 (Fig. 8d).

Since each pair of slabs provides four surfaces for testing (therefore, two contacts), it is possible to study the differences between the  $\beta$  values obtained in the two available

contacts of the same pair of slabs under a specific moisture condition. This analysis, which is shown in Table 4, indicates that these differences in  $\beta$  values are frequently smaller than the maximum standard deviation of  $\beta$  obtained in a unique contact and lesser than  $4^\circ$  (or 11% of the mean value), except for some pair of slabs of S-1 and S-2 tested in fully water-saturated state. As a consequence, it confirms that tilt tests may be performed using the two surfaces provided by each slab with the aim to increase the number of  $\beta$  values available. Nevertheless, having a uniform surface finish of the specimens is essential when proceeding in this way since the aforementioned exception found in some pairs of slabs could be attributed to the existence of undesirable surface irregularities generated during saw cutting of the specimens.

The impact of wear on the sliding angle is another interesting aspect to be analysed. For this purpose, the variations of  $\beta$  values of tested limestones with the number of tilt test repetitions in dry condition, fully water-saturated state and under exposure to an environmental RH equal to 90% have been depicted using boxplots in Fig. 9a, b and c, respectively. These graphs show that the differences between the  $\beta$  values measured in each repetition are trivial and data do not follow any clear tendency. In other words,

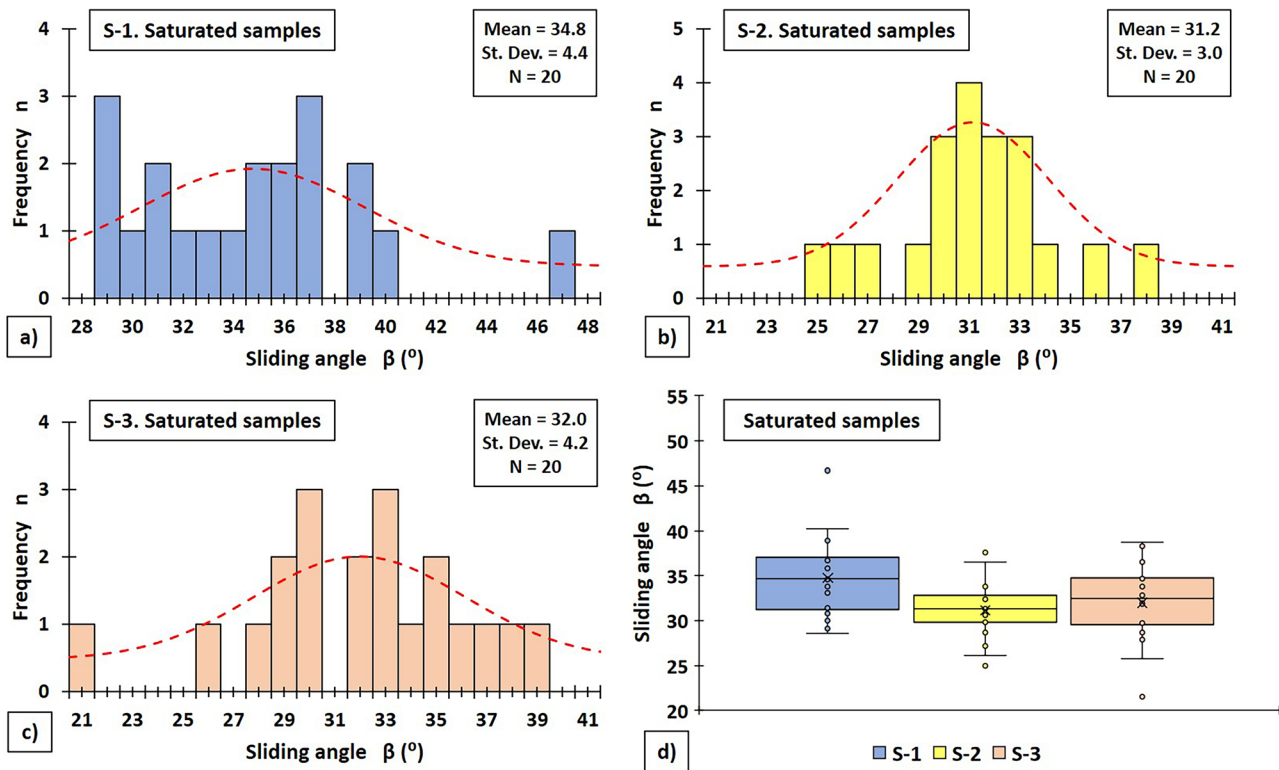


**Fig. 7** Histograms showing sliding angle values for five repetition of tilt tests conducted on four contact surfaces of S-1 (a), S-2 (b) and S-3 (c) under fully water-saturated conditions and the correspond-

ing box and whisker plots comparing the results obtained in the three tested limestones. Dashed lines represent the fitted normal distribution

the hypothetical lines of fit between  $\beta$  and the numbers of repetitions are practically horizontal, which suggests that there is no relationship of dependence between the two variables for the studied rocks and five test repetitions. Therefore, this finding indicates that, if only five repetitions of the tilt test are performed on the same pair of rock surfaces and the debris generated by friction is removed between each repetition, the  $\beta$  value of tested limestones is not significantly affected by wear.

A comparison of the  $\beta$  values measured in tested rocks in dry, fully water-saturated conditions and under exposure to an environmental RH equal to 90% using boxplots is shown in Fig. 9d. Full water saturation resulted in an average  $\beta$  increase of 9% in the calcarenite S-1 compared to the dry state. However, the opposite effect was observed for the other two varieties. In particular,  $\beta$  reductions of 17% were obtained for calcarenite S-2 and of 13% for calcarenite S-3. Exposure to an environmental RH of 90% caused small  $\beta$  variations in the three lithotypes. Specifically, an average  $\beta$  increase of 3% was obtained in calcarenite S-1, almost negligible change was observed in calcarenite S-2 (an increase of 1%) and a decrease of 3% was found in calcarenite S-3.

### Basic friction angle under different testing conditions

Basic friction angle ( $\phi_b$ ) values of each pair of tested contact surfaces calculated using the Eq. (5) as well as the corresponding mean values ( $\bar{\phi}_b$ ) and standard deviations ( $\sigma_{\phi_b}$ ) are listed in Table 5.

In dry conditions, calcarenite S-1 displayed the lowest  $\phi_b$  values, with numbers varying between 29.7 and 34.3°, a mean value of 32.0° and a standard deviation of 1.6°. The other calcarenites (S-2 and S-3) showed close values to each other although a larger variability was obtained in S-2. In particular,  $\phi_b$  values were in the range of 34.9–40.8° in S-2 and of 35.0–38.4 in S-3, the mean values were 37.4° in S-2 and 37.2° in S-3 and the standard deviations were 2.1° in S-2 and 1.3° in S-3.

In fully water-saturated conditions, calcarenite S-1 exhibited the highest  $\phi_b$  values, with figures ranging between 30.8 and 37.0°, a mean value of 34.1° and a standard deviation of 2.8°. On the contrary, calcarenite S-2 showed the smallest  $\phi_b$  values, with figures fluctuating between 27.2 and 32.8°, a mean value of 30.5° and a standard deviation of 2.1°. With respect to calcarenite S-3, it displayed  $\phi_b$  values varying between 31.9 and 34.7°, a mean value of 33.0° and

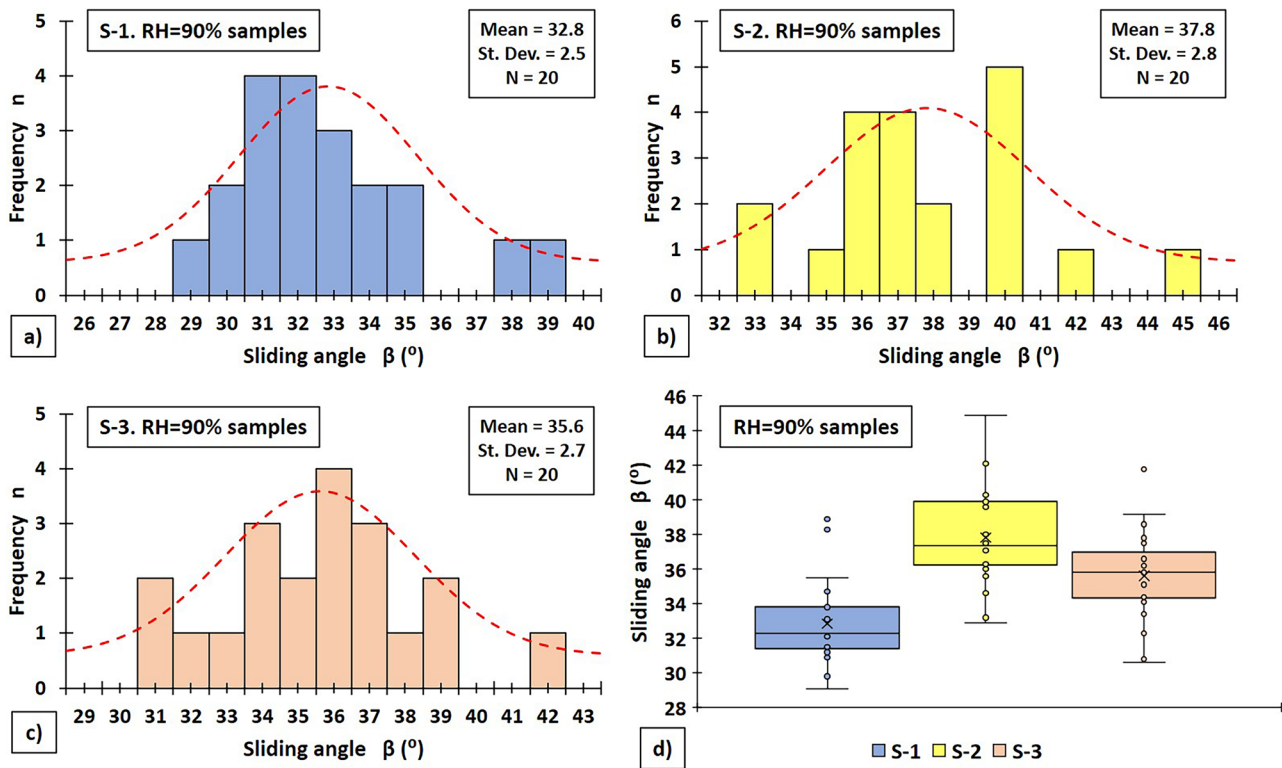


**Fig. 8** Histograms showing sliding angle values for five repetition of tilt tests conducted on four contact surfaces of S-1 (a), S-2 (b) and S-3 (c) under a controlled environmental RH equal to 90% and the

corresponding box and whisker plots comparing the results obtained in the three tested limestones. Dashed lines represent the fitted normal distribution

a standard deviation of 1.1°. At this point, it should be highlighted that S-1 presented a much more marked dispersion under this testing condition than the other lithotypes, and especially greater than S-3.

Regarding the specimens subjected to an environmental RH of 90%, calcarenite S-2 showed the biggest  $\varphi_b$  values, with numbers varying from 37.1 to 39.6°, a mean value of 37.9° and a standard deviation of 1.0°. In contrast, calcarenite S-1 presented the lowest  $\varphi_b$  values, with figures ranging between 31.2 and 35.5°, a mean value of 32.8° and a standard deviation of 1.6°. In calcarenite S-3, the  $\varphi_b$  values

fluctuated among 34.4 and 37.8, the mean value was 35.9° and the standard deviation was 1.4°.

In Fig. 10 can be seen the box and whiskers plots comparing the  $\varphi_b$  values obtained in the three limestone varieties under the three different moisture conditions. This graph reveals that fully water-saturated samples generally exhibit greater variability of  $\varphi_b$  than dry specimens and those subjected to an environmental RH = 90%. Calcarenite S-1 experienced a moderate  $\varphi_b$  increase (6%) while S-2 and S-3 suffered substantial  $\varphi_b$  reductions (18 and 11%, respectively) due to water saturation. Particularly, the ratio

**Table 4** Differences in the sliding angle ( $\beta$ ) values obtained in the two available contacts of the same pair of slabs in dry, fully water condition and under exposure to a RH equal to 90%

Rock type	Dry condition				Saturated condition				Exposure to RH=90%			
	Pair of slab	Difference in $\beta$		Pair of slab	Difference in $\beta$		Pair of slab	Difference in $\beta$				
		(°)	(%)		(°)	(%)		(°)	(%)			
S-1	1–2	2.0	6.1	5–6	6.7	19.4	9–10	3.4	10.1			
	3–4	2.9	9.6	7–8	5.1	14.6	11–12	0.4	1.3			
S-2	1–2	2.6	7.1	5–6	4.3	14.0	9–10	2.1	5.5			
	3–4	3.7	9.5	7–8	2.1	6.5	11–12	0.2	0.6			
S-3	1–2	2.1	5.8	5–6	1.8	5.6	9–10	1.9	5.4			
	3–4	0.4	1.2	7–8	0.1	0.3	11–12	2.9	8.3			



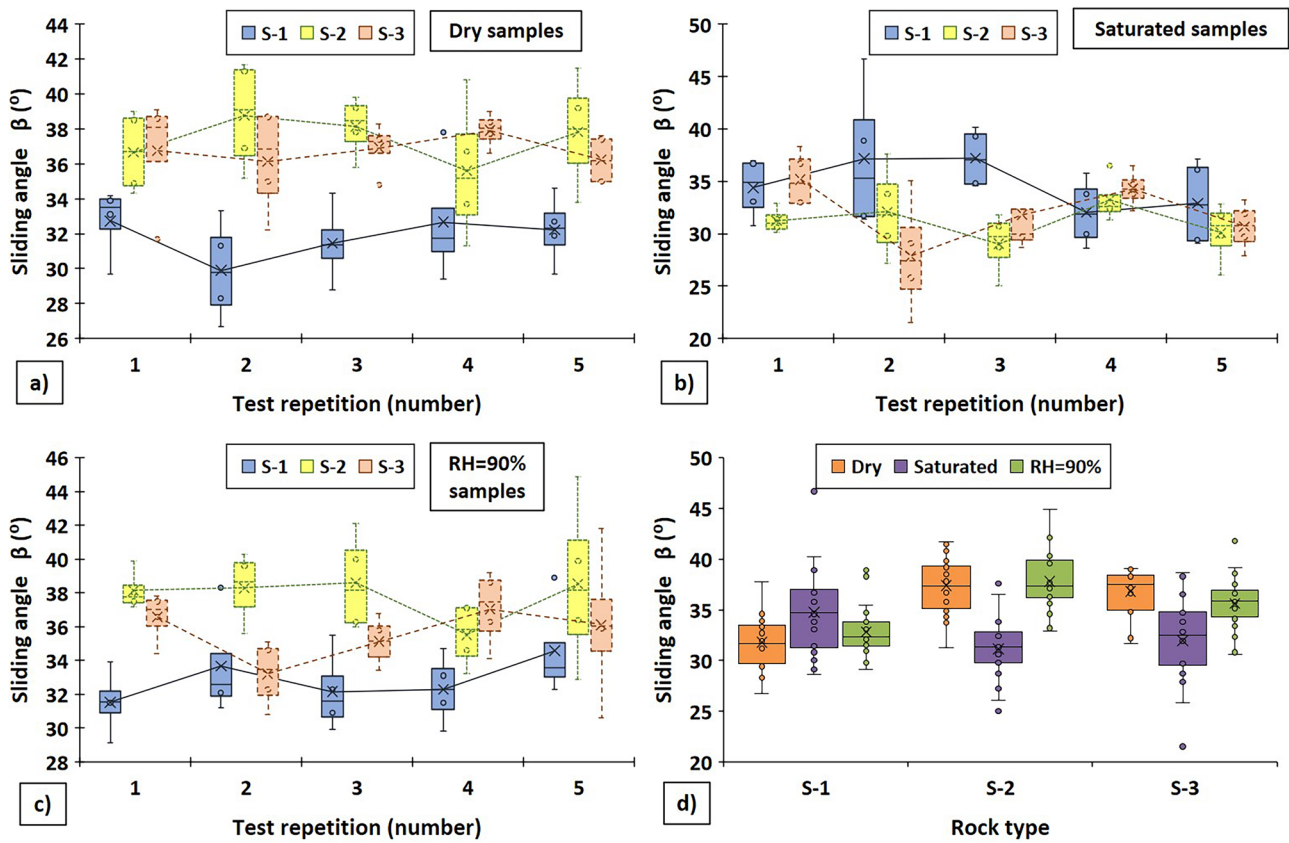


**Fig. 9** Variations of sliding angle ( $\beta$ ) values of tested limestones with the number of tilt test repetitions in dry condition (a), fully water-saturated state (b) and under exposure to an environmental RH=90% (c)

and comparison of  $\beta$  values measured in tested rocks under different moisture conditions (d)

between the  $\mu$  ( $\tan \phi_b$ ) values measured in fully water-saturated and dry states ( $K_{sd} = \tan(\overline{\phi_{bsat}})/\tan(\overline{\phi_{bdry}})$ ) was 1.08 in S-1, 0.77 in S-2 and 0.86 in S-3. Calcarenites S-1 and S-2 underwent small  $\phi_b$  increases (3 and 1%, respectively) whereas S-3 suffered a slight  $\phi_b$  decrease (3%) when exposed to high RH. Concretely, the ratio between the  $\mu$  values obtained under an environmental RH equal to 90% and dry condition ( $K_{hd} = \tan(\overline{\phi_{bRH=90\%}})/\tan(\overline{\phi_{bdry}})$ ) was 1.03 in S-1, 1.02 in S-2 and 0.96 in S-3.

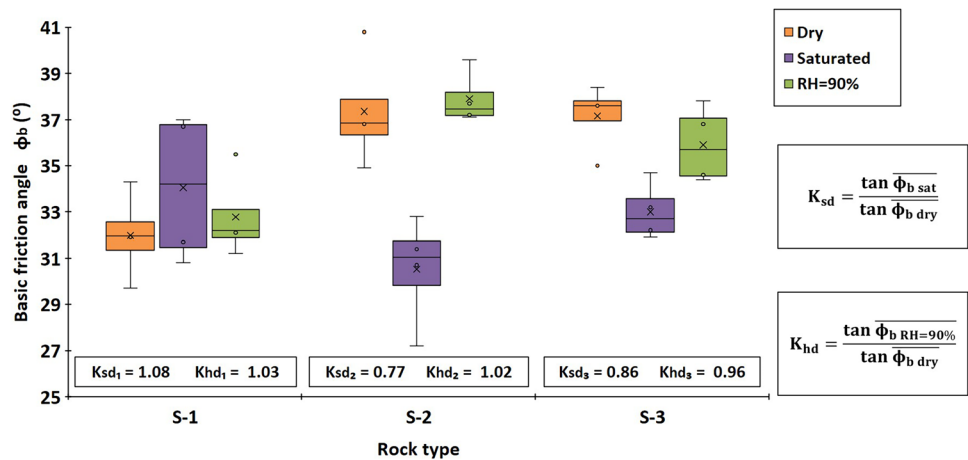
**Relationships between petrological characteristics and microstructure of tested calcarenites, basic friction angle and water-induced changes**

The  $\phi_b$  values of the tested rocks and their water-induced changes are related to their petrological characteristics and microstructure. In dry state, calcarenite S-1, which presents the smallest mean grain size ( $M_z$ ), exhibited a considerably lower  $\phi_b$  value than calcarenites S-2 and S-3, which

**Table 5** Basic friction angles ( $\phi_{bk}$ ) obtained in every tested contact (k) of the three rocks under the three different moisture conditions and the corresponding mean values ( $\overline{\phi_b}$ ) and standard deviations ( $\sigma_{\phi_b}$ )

Rock type (condition)	$\phi_{b1}$ (°)	$\phi_{b2}$ (°)	$\phi_{b3}$ (°)	$\phi_{b4}$ (°)	$\overline{\phi_b}$ (°)	$\sigma_{\phi_b}$ (°)
S-1 (Dry)	31.9	34.3	29.7	32.0	32.0	1.6
S-2 (Dry)	36.8	34.9	40.8	36.9	37.4	2.1
S-3 (Dry)	35.0	37.6	37.6	38.4	37.2	1.3
S-1 (fully water-saturated)	37.0	30.8	36.7	31.7	34.1	2.8
S-2 (fully water-saturated)	32.8	27.2	30.7	31.4	30.5	2.1
S-3 (fully water-saturated)	32.2	34.7	33.2	31.9	33.0	1.1
S-1 (RH=90%)	32.3	35.5	32.1	31.2	32.8	1.6
S-2 (RH=90%)	37.2	39.6	37.1	37.7	37.9	1.0
S-3 (RH=90%)	34.6	36.8	37.8	34.4	35.9	1.4

**Fig. 10** Box and whiskers plots comparing the basic friction angle ( $\phi_b$ ) values obtained in tested limestones in dry, fully water-saturated conditions and under exposure an environmental RH of 90%



have larger  $M_z$  (Fig. 11a). Furthermore, it was found that calcarenites S-2 and S-3, which present a higher content of clay minerals (i.e. phyllosilicates) as well as a significantly greater total porosity ( $p$ ) and pore diameter ( $d_M$ ), displayed  $\phi_b$  reductions due to water saturation (Fig. 11b, c, d). In contrast, calcarenite S-1, which has a scarce content of clay minerals, and smaller  $p$  and  $d_M$  values exhibited a  $\phi_b$  increase when saturated (Fig. 11b, c, d).

### Discussion

In this work, the petrological and microstructural characteristics as well as the sliding angle ( $\beta$ ) values of three lithotypes of porous limestones under dry and saturated conditions, as well as after an exposition to an environment of high relative humidity (RH), have been determined by performing a large number of tilt tests. The

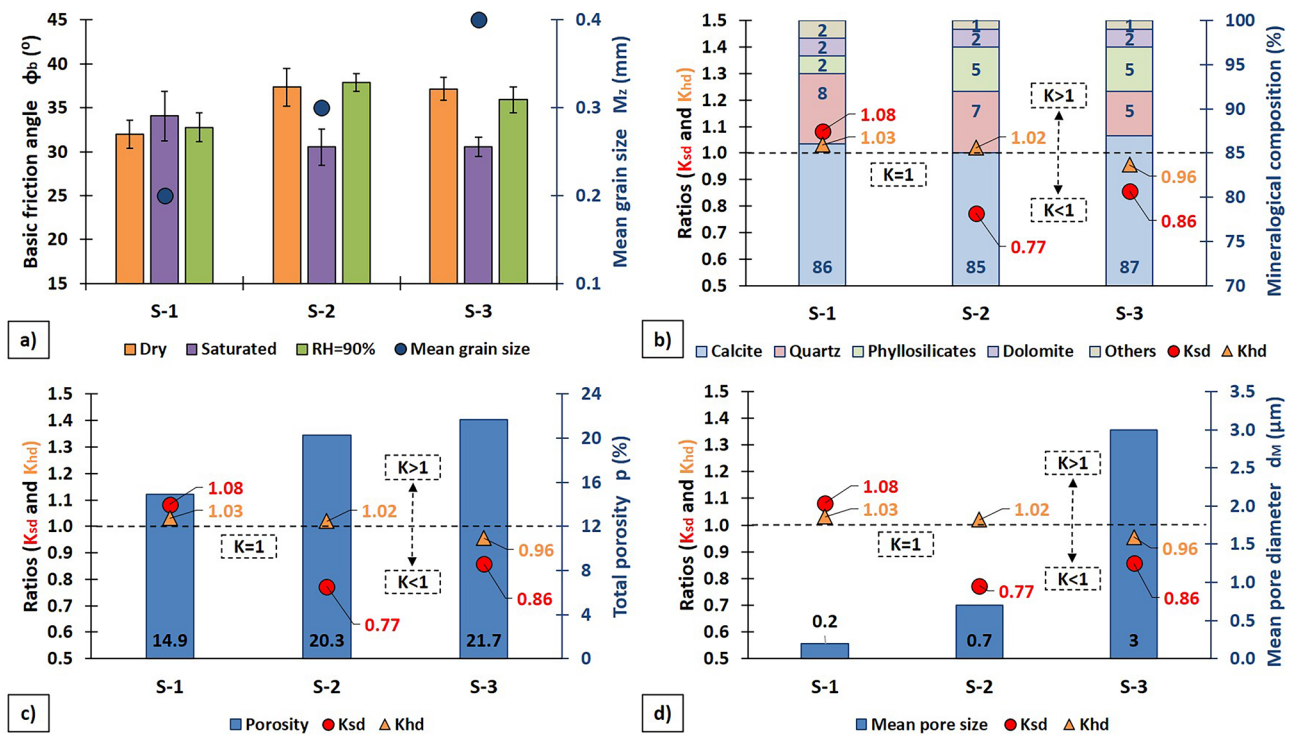


**Fig. 11** (a) Relationships between the basic friction angle ( $\phi_b$ ) of tested limestones and the mean grain size ( $M_z$ ); relationship among the ratios  $K_{sd}$  and  $K_{hd}$  and (b) their mineralogical composition; (c) their total porosity ( $p$ ); and (d) their mean pore diameter ( $d_M$ ).

results obtained have allowed to (1) evaluate the possible impact of the repetition of tilt test conducted on the same rock contact (a pair of rock surfaces) on  $\beta$ ; (2) quantify the effect of water saturation and environmental RH on the basic friction angle ( $\varphi_b$ ) value of these rocks; and (3) establish connections between properties such as grain size, mineralogical composition, porosity or pore size and  $\varphi_b$  or its moisture-induced variations. The obtained results are compared with those reported in previous investigations and their implications and limitations are discussed below.

A first finding of this work is that the  $\beta$  values obtained under dry conditions exhibited moderate standard deviations (always less than  $3^\circ$ ) while the  $\beta$  values measured under fully water-saturated conditions displayed considerably higher standard deviations (between  $3$  and  $4.2^\circ$ ). This result is in line with those obtained by Ulusay and Karakul (2016) in Turkish rocks and by Zhang et al. (2018) in Norwegian rocks, who reported that standard deviations were often greater in saturated specimens than in dry ones. This may be explained because water distribution on saturated slab surfaces is unavoidably slightly different for each test repetition and powder generated during sliding is more difficult to remove completely in this case. In addition, the standard deviations obtained in both conditions are generally higher than those informed in the previously cited studies, which may be attributed to the fact that they refined the raw data by discarding the maximum and minimum  $\beta$  values before their calculation. The standard deviations of  $\beta$  found in the sets of samples exposed to an RH equal to 90% were moderate (less than  $3^\circ$ ) and quite similar to those obtained under dry conditions. This occurred despite the fact that the special test setup used on these specimens required to stop the tilting table in a manual way when sliding started (i.e. not automatically as in the dry and fully water-saturated specimens). This fact can be explained by the fast and efficient work of the laboratory operators in detecting the onset of sliding and stopping the tilting table, as well as by the low tilting velocity used during the tests ( $10^\circ/\text{min}$ ). In this sense, it is worth mentioning that a one-second variation in the reaction time of the operators to stop the tilting table would result in a variation of the measured  $\beta$  of less than  $0.2^\circ$ .

A second outcome of this study is the existence of several outliers in the  $\beta$  values obtained in the three limestones tested under different moisture conditions, as revealed by the box-and-whisker plots. This fact shows the recommendation proposed by Alejano et al. (2012a) to use the median of  $\beta$  values instead of the mean to determine a representative  $\varphi_b$  value, which has been included in the recently published ISRM Suggested Method (Alejano et al. 2018). Nevertheless, according to Gonzalez et al. (2014), the mean  $\beta$  value of the five first tests conducted on freshly saw-cut samples could also be used as the input

$\varphi_b$  parameter in the Barton's model to realistically estimate the shear strength of unfilled discontinuities. In addition, the present investigation corroborates that tilt tests could be carried out using the two surfaces of each rock slab in order to have a larger number of  $\beta$  values from which to derive a representative  $\varphi_b$ , given that both rock surfaces are homogeneous and free of irregularities. The latter is not always easy to achieve in soft rocks such as tested limestones, despite the availability of modern cutting tools and skilled operators.

Furthermore, our tilt test results indicate that  $\beta$  values of calcarenites are not significantly affected by wear when only five test repetitions are conducted on the same rock contact and the debris generated by friction is removed between each repetition, which is consistent with the findings reported by Ulusay and Erguler (2016). Notwithstanding the foregoing, previous works have demonstrated that repeated tilt testing of saw-cut specimens could cause a  $\beta$  reduction when the rock debris is removed after every test repetition and a  $\beta$  increase when the rock debris is not removed (Hencher 1976, 2012; González et al. 2014; Pérez-Rey et al. 2015, 2016; Alejano et al. 2017). In this connection, Kasyap and Senetakis (2018) found that the debris scraped during micro-mechanical shearing tests could contribute to the increase of friction of kaolinite-coated sand grains. Also, Ren et al. (2022) suggested that the variations of the interface friction of miniature kaolinite specimens are strongly related with abrasion and the presence of water. In particular, they observed that the increase of shearing cycles leads to a slight increase of the interface friction in dry condition and, on the contrary, an important reduction of the interface friction in wet state. Therefore, although the level of normal stresses in tilt tests is very small, the choice of an appropriate number of test repetitions performed on the same rock contact could be an important matter to consider when conducting tilt tests, especially on weak rocks.

A third result of this research is that the  $\varphi_b$  values of tested calcarenites are in a range of  $31.2$ – $37.8$ , which are comparable to those obtained by other researchers in similar sedimentary rocks, such as dolomite ( $27$ – $37^\circ$ ), limestone ( $35$ – $40^\circ$ ) (Coulson 1972) or travertines ( $28.2$ – $38.3^\circ$ ) (Ulusay and Karakul 2016). Furthermore, in the dry state, the  $\varphi_b$  value found in calcarenite S-1 ( $31.8^\circ$ ) was lower than those measured in calcarenites S-2 and S-3 ( $37.4$  and  $36.8^\circ$ , respectively), which can be explained by its smaller grain size. This fact has also been noted by Cruden and Hu (1988), who reported that large grain sizes increase  $\varphi_b$  in Canadian pure carbonate rocks.

A fourth finding of this work is that moisture can cause both positive and negative  $\varphi_b$  increments in calcarenites. The  $\varphi_b$  increase of 6% obtained in calcarenite S-1 after its fully water-saturation could be attributed to the fact that in this variety, the capillary (suction) effect prevails over

the lubrication effect (Ulusay and Karakul 2016). Previous research has found analogous  $\phi_b$  increases in some sedimentary (i.e. sandstone, limestone and travertine) and volcanic (andesite granite, diorite and gabbro) rocks (Ulusay and Karakul 2016; Zhang et al. 2018; Kim and Jeon 2019). In contrast, the  $\phi_b$  reductions of 18 and 11% obtained in the calcarenites S-2 and S-3 could be attributed to the occurrence of the opposite phenomenon, that is the dominance of the lubrication over the capillary effect (Ulusay and Karakul 2016). Similar  $\phi_b$  decreases have been found by other academics in several types of sedimentary (sandstone, dolomite and limestone), metamorphic (slate and marble) and volcanic (basalt, granite, dolerite, pegmatite and migmatite) rocks (Coulson 1972; Richards 1975; Ulusay and Karakul 2016; Zhang et al. 2018).

In this connection, the different impact of water saturation on  $\phi_b$  obtained in tested limestones may be related to the differences in their microstructure and mineralogical composition. On the one hand, the smaller pore and grain size of the calcarenite S-1 would promote the accumulation of water molecules on the voids of rock surface and their permanence despite its drying with a cloth just before conducting tilt tests. However, the larger grain and pore sizes of calcarenites S-2 and S-3 would cause a more effective removal of the water molecules lodged in the voids of the rock surface when wiping it with the cloth. Consequently, the effect of surface tension would be considerably more substantial in calcarenite S-1 than in the others. On the other hand, the higher content of clay minerals (phyllosilicates) and the lower quartz content of the calcarenites S-2 and S-3 compared to the calcarenite S-1 might be other reason to explain the dissimilar water-induced changes of  $\phi_b$  found in each lithotype. In this line, former basic research has demonstrated that moisture caused important drops of the  $\mu$  in clayey and sheet-structure minerals (e.g. chlorite, lizardite, kaolinite, talc and biotite) and slight increase or no change in minerals with a massive structure (e.g. calcite, quartz and feldspar) (Horn and Deere 1962; Morrow et al. 2000; Moore and Lockner 2004). In addition, the higher water-induced variations in  $\phi_b$  exhibited by calcarenites S-2 and S-3 compared to S-1 may be related to their larger water absorption capacity, as well as to the fact that S-1 had greater mechanical properties and displayed a sparry and siliceous fibrous cement that makes its grains better cemented.

The variations of  $\phi_b$  with environmental RH were slight in the three tested limestones. In particular, when the RH varied from 50 to 90%, the  $\phi_b$  increased by 3% in calcarenite S-1 and by 1% in calcarenite S-2, while  $\phi_b$  decreased by 3% in calcarenite S-3. These minor changes can be attributed to the small amount of water adsorbed by these rocks (0.64–1.08%) and its homogeneous distribution within the pores when subjected to the humidity chamber atmosphere. Therefore, to know the  $\phi_b$  values of this rock types under RH

conditions to which rock masses are commonly exposed, it is not necessary to conduct the test in a precise (and more complex) way, since the differences with the dry  $\phi_b$  values are very small. Nevertheless, its generalisation for all rock types requires further research. In this sense, Westbrook and Jorgensen (1968) found that crystal planes of some synthetic minerals (i.e. bromellite, periclase, corundum, rutile and silicon carbide) and natural minerals (quartz, kyanite, topaz, tourmaline, fluorite, sphalerite, galena and calcite) exhibited substantial drops (up to 32%) in their relative values of the indentation microhardness due to water adsorption from ambient air. Also, Macmillan et al. (1974) postulated that the increment in the  $\mu$  of glass in wet environments could be attributed to chemically induced variations in surface microhardness.

## Conclusions

Based on the experimental work and the analyses carried out in the present article, the following conclusions can be derived:

- (1) The standard deviations of  $\beta$  values found in calcarenites tested in fully water-saturated state were substantially greater than those measured in dry condition or under exposure to an environmental RH of 90%. This finding could be attributed to the fact that water distribution on saturated rock surfaces was inevitably slightly dissimilar for each test repetition. Furthermore, due to the greater difficulty in achieving an effective debris removal from rock surfaces in water-saturated specimens, undesired dust generated during sliding may remain adhered to their rock surface in some tests, which could also justify the higher  $\beta$  variability observed in them.
- (2) The  $\beta$  values of calcarenites were not importantly affected by wear when only five test repetitions were conducted on the same rock contact and the powder generated during sliding was removed between repetitions. Furthermore, the differences between the mean  $\beta$  values obtained in each contact of the same pair of slabs were not significant, so tilt tests might be performed using the two surfaces provided by each slab with the aim to increase the number of available data. However, some  $\beta$  datasets have outliers and did not fit well to a normal distribution, so using the median of  $\beta$  values instead of the mean would be recommended to obtain a characteristic  $\phi_b$  value.
- (3) Full water saturation caused both positive and negative  $\phi_b$  increments in calcarenites. In particular, a  $\phi_b$  increase of 6% was obtained in calcarenite S-1 while  $\phi_b$  reductions of 18% and 11% were found in calcar-



enites S-2 and S-3, respectively. This finding could be attributed to the prevalence of capillary effect over lubrication effect in S-1 whereas just the contrary happened in S-2 and S-3, which can be explained by their differences in microstructure and mineralogy. Exposure to a high environmental RH of 90% caused minor  $\phi_b$  changes in the three limestone lithotypes (of around 3%), which could be justified by the small amount of water adsorbed on rock surfaces (less than 1.1%) that homogeneously distributes within the pore walls. Therefore, the development of the tilt test under different RH conditions does not appear to be strictly necessary for the studied calcareous rocks due to the small effect on friction angles caused by the low changes in moisture content achieved by the vapour equilibrium technique.

This study offers an in-depth understanding of the influence of water saturation and environmental RH on the  $\phi_b$  of porous limestones that may be of interest for the design and execution of infrastructures (e.g. dams, ports, tunnels, mines and nuclear waste repositories) built in or on rock masses in which water or RH can play an important role in their stability. Furthermore, the findings related to the effect of wear and moisture on  $\beta$  values as well as its variability provide valuable knowledge that can serve as reference on how to perform tilt tests on porous calcareous rocks.

**Acknowledgements** The authors thank the company “Bateig Piedra Natural S.A.” for providing the rock samples. The authors would also like to express their gratitude to the Earth Sciences Department from the University of Alicante for allowing us to perform the thin-sections analysis in its laboratory.

**Funding** Open Access funding provided thanks to the CRUE-CSIC agreement with Springer Nature. This work was partially supported by the Vicerrectorado de Investigación y Transferencia del Conocimiento of the University of Alicante through the projects UAUSTI18-21, UAUSTI20-20 and UAUSTI19-25.

## Declarations

**Competing interests** The authors declare no competing interests.

**Open Access** This article is licensed under a Creative Commons Attribution 4.0 International License, which permits use, sharing, adaptation, distribution and reproduction in any medium or format, as long as you give appropriate credit to the original author(s) and the source, provide a link to the Creative Commons licence, and indicate if changes were made. The images or other third party material in this article are included in the article’s Creative Commons licence, unless indicated otherwise in a credit line to the material. If material is not included in the article’s Creative Commons licence and your intended use is not permitted by statutory regulation or exceeds the permitted use, you will need to obtain permission directly from the copyright holder. To view a copy of this licence, visit <http://creativecommons.org/licenses/by/4.0/>.

## References

- Alejano LR, Ferrero AM, Ramírez-Oyanguren P, Álvarez Fernández MI (2011) Comparison of limit-equilibrium, numerical and physical models of wall slope stability. *Int J Rock Mech Min Sci* 48:16–26. <https://doi.org/10.1016/j.ijrmms.2010.06.013>
- Alejano LR, Gómez-Márquez I, Martínez-Alegría R (2010) Analysis of a complex toppling-circular slope failure. *Eng Geol* 114:93–104. <https://doi.org/10.1016/j.enggeo.2010.03.005>
- Alejano LR, González J, Muralha J (2012a) Comparison of different techniques of tilt testing and basic friction angle variability assessment. *Rock Mech Rock Eng* 45:1023–1035. <https://doi.org/10.1007/s00603-012-0265-7>
- Alejano LR, Muralha J, Ulusay R et al (2018) ISRM Suggested Method for Determining the Basic Friction Angle of Planar Rock Surfaces by Means of Tilt Tests. *Rock Mech Rock Eng* 51:3853–3859. <https://doi.org/10.1007/s00603-018-1627-6>
- Alejano LR, Muralha J, Ulusay R et al (2017) A benchmark experiment to assess factors affecting tilt test results for sawcut rock surfaces. *Rock Mech Rock Eng* 50:2547–2562. <https://doi.org/10.1007/s00603-017-1271-6>
- Alejano LR, Taboada J, García-Bastante F, Rodríguez P (2008) Multi-approach back-analysis of a roof bed collapse in a mining room excavated in stratified rock. *Int J Rock Mech Min Sci* 45:899–913. <https://doi.org/10.1016/j.ijrmms.2007.10.001>
- Alejano LR, Veiga M, Gómez-Márquez I, Taboada J (2012b) Stability of granite drystone masonry retaining walls: II. Relevant parameters and analytical and numerical studies of real walls. *Geotechnique* 62:1027–1040. <https://doi.org/10.1680/geot.10.P.113>
- Aydan Ö (1995) A portable system for in situ characterization of surface morphology and frictional properties of rock discontinuities. In: SGEEditoriali (ed) *Field Measurements in Geomechanics: Proceedings of 4th International Symposium*. Bergamo, Italy, pp 463–470
- Barton N (1971) Estimation of in situ shear strength from back analysis of failed rock slopes. In: *Proc Int Symp Rock Mech Nancy*, pp II–27
- Barton N (1973) Review of a new shear-strength criterion for rock joints. *Eng Geol* 7:287–332. [https://doi.org/10.1016/0013-7952\(73\)90013-6](https://doi.org/10.1016/0013-7952(73)90013-6)
- Barton N, Choubey V (1977) The shear strength of rock joints in theory and practice. *Rock Mech* 10:1–54. <https://doi.org/10.1007/BF01261801>
- Barton NR (2011) From empiricism, through theory, to problem solving in rock engineering. 6th Leopold Müller Lecture. In: Qian Q, Zhou Y (eds) *12th ISRM International Congress on Rock Mechanics: Harmonising Rock Engineering and the Environment*. CRC Press, Beijing, China, pp 1–14
- Beyhan S, Özdemir M (2021) Evaluation of the basic friction angle in dry and conditioned fluids by tilt tests. In: *IOP Conference Series: Earth and Environmental Science*. p 012028
- Coulomb CA (1766) *Essai sur une application des règles de maximis & minimis à quelques problèmes de statique, relatifs à l’architecture*. In: *Mémoires de Mathématique et de Physique*. pp 343–383
- Coulson JH (1972) Shear strength of flat surfaces in rock. Stability of rock slopes. In: Cording EJ (ed) *Proceedings of 13th Symposium on Rock Mechanics*. American Society of Civil Engineers, New York, pp 77–105
- Cruden DM, Hu XQ (1988) Basic friction angles of carbonate rocks from Kananaskis country, Canada. *Bull Int Assoc Eng Geol* 38:55–59. <https://doi.org/10.1007/BF02590448>
- Fort R, Bernabéu A, García del Cura MA et al (2010) La Piedra de Novelda: una roca muy utilizada en el patrimonio arquitectónico. *Mater Construcción* 52:19–32. <https://doi.org/10.3989/mc.2002.v52.i266.332>



- Ghazvinian AH, Azinfar MJ, Geranmayeh Vaneghi R (2012) Importance of tensile strength on the shear behavior of discontinuities. *Rock Mech Rock Eng* 45:349–359. <https://doi.org/10.1007/s00603-011-0207-9>
- González J, González-Pastoriza N, Castro U et al (2014) Considerations on the laboratory estimate of the basic friction angle of rock joints. In: Alejano LR, Peruchó A, Olalla C, Jiménez R (eds) *Rock Engineering and Rock Mechanics: Structures in and on Rock Masses - Proceedings of EUROCK 2014, ISRM European Regional Symposium*. Vigo, Spain, pp 199–204
- Gutierrez M, Øino L, Høeg K (2000) The effect of fluid content on the mechanical behaviour of fractures in chalk. *Rock Mech Rock Eng* 33:93–117. <https://doi.org/10.1007/s006030050037>
- Hencher SR (1976) Discussion: a simple sliding apparatus for the measurement of rock joint friction. *Géotechnique* 26:641–644. <https://doi.org/10.1680/geot.1976.26.4.641>
- Hencher SR (2012) Discussion of the paper “‘comparison of different techniques of tilt testing and basic friction angle variability assessment”’. *Rock Mech Rock Eng* 45:1137–1139. <https://doi.org/10.1007/s00603-012-0288-0>
- Hencher SR (1977) The effect of vibration on the friction between planar rock surfaces. *Imperial Collegue of Science and Technology*
- Hencher SR, Richards LR (2015) Assessing the shear strength of rock discontinuities at laboratory and field scales. *Rock Mech Rock Eng* 48:883–905. <https://doi.org/10.1007/s00603-014-0633-6>
- Horn HM, Deere DU (1962) Frictional Characteristics of Minerals. *Géotechnique* 12:319–335. <https://doi.org/10.1680/geot.1962.12.4.319>
- Hoskins ER, Jaeger JC, Rosengren KJ (1968) A medium-scale direct friction experiment. *Int J Rock Mech Min Sci* 5:143–154. [https://doi.org/10.1016/0148-9062\(68\)90030-2](https://doi.org/10.1016/0148-9062(68)90030-2)
- Jaeger JC (1959) The frictional properties of joints in rock. *Geofis Pura e Appl* 43:148–158. <https://doi.org/10.1007/BF01993552>
- Jang HS, Zhang QZ, Kang SS, Jang BA (2018) Determination of the basic friction angle of rock surfaces by tilt tests. *Rock Mech Rock Eng* 51:989–1004. <https://doi.org/10.1007/s00603-017-1388-7>
- Kasyap SS, Senetakis K (2018) A micromechanical experimental study of kaolinite-coated sand grains. *Tribol Int* 126:206–217. <https://doi.org/10.1016/j.triboint.2018.05.021>
- Kasyap SS, Senetakis K (2020) An experimental investigation on the tribological behaviour of nominally flat quartz grains with gouge material in dry, partial saturated and submersed conditions. *Pure Appl Geophys* 177:3283–3300. <https://doi.org/10.1007/s00024-020-02431-1>
- Kasyap SS, Senetakis K (2021) Micromechanical-based experimental and analytical studies on rate effects and stick-slip instability of smooth quartz surfaces in the presence of plastic and non-plastic gouges. *Int J Numer Anal Methods Geomech* 45:776–793. <https://doi.org/10.1002/nag.3178>
- Kim DH, Gratchev I, Hein M, Balasubramaniam A (2016) The application of normal stress reduction function in tilt tests for different block shapes. *Rock Mech Rock Eng* 49:3041–3054. <https://doi.org/10.1007/s00603-016-0989-x>
- Kim T, Jeon S (2019) Experimental study on shear behavior of a rock discontinuity under various thermal, hydraulic and mechanical conditions. *Rock Mech Rock Eng* 52:2207–2226. <https://doi.org/10.1007/s00603-018-1723-7>
- Kveldsvik V, Nilsen B, Einstein HH, Nadim F (2008) Alternative approaches for analyses of a 100,000 m<sup>3</sup> rock slide based on Barton-Bandis shear strength criterion. *Landslides* 5:161–176. <https://doi.org/10.1007/s10346-007-0096-x>
- Li CC, Zhang N, Ruiz J (2019) Measurement of the basic friction angle of planar rock discontinuities with three rock cores. *Bull Eng Geol Environ* 78:847–856. <https://doi.org/10.1007/s10064-017-1045-0>
- Li Z, Sheng Y, Reddish DJ (2005) Rock strength reduction and its potential environmental consequences as a result of groundwater rebound. In: 9th International Mine Water Congress. pp 513–519
- Macmillan NH, Huntington RD, Westwood ARC (1974) Chemomechanical control of sliding friction behaviour in non-metals. *J Mater Sci* 9:697–706. <https://doi.org/10.1007/BF00761789>
- Mehrishal S, Sharifzadeh M, Shahriar K, Song JJ (2016) An experimental study on normal stress and shear rate dependency of basic friction coefficient in dry and wet limestone joints. *Rock Mech Rock Eng* 49:4607–4629. <https://doi.org/10.1007/s00603-016-1073-2>
- Misra A, Marangos O (2011) Rock-joint micromechanics: relationship of roughness to closure and wave propagation. *Int J Geomech* 11:431–439. [https://doi.org/10.1061/\(asce\)gm.1943-5622.0000021](https://doi.org/10.1061/(asce)gm.1943-5622.0000021)
- Moore DE, Lockner DA (2004) Crystallographic controls on the frictional behavior of dry and water-saturated sheet structure minerals. *J Geophys Res* 109:1–16. <https://doi.org/10.1029/2003JB002582>
- Morrow CA, Moore DE, Lockner DA (2000) The effect of mineral bond strength and adsorbed water on fault gouge frictional strength. *Geophys Res Lett* 27:815–818. <https://doi.org/10.1029/1999GL008401>
- Ordóñez S, Fort R, Garcia del Cura MA (1997) Pore size distribution and the durability of a porous limestone. *Q J Eng Geol* 30:221–230. <https://doi.org/10.1144/GSL.QJEG.1997.030.P3.04>
- Ordóñez S, Louis M, García del Cura MA et al (1994) Physical properties and petrographic characteristics of some Bateig stone varieties. In: Oliveira R, Rodrigues AG, Coelho AG, Cunha AP (eds) 7th International IAEG Congress. Lisboa, pp 3595–3603
- Patton FD (1966) Multiple modes of shear failure in rock and related materials. University of Illinois
- Pellet FL, Keshavarz M, Boulon M (2013) Influence of humidity conditions on shear strength of clay rock discontinuities. *Eng Geol* 157:33–38. <https://doi.org/10.1016/j.enggeo.2013.02.002>
- Pérez-Rey I (2019) Study of the frictional behaviour of planar saw-cut rock surfaces towards a methodology for tilt testing and its application to case studies. University of Vigo
- Pérez-Rey I, Alejano LR, Arzúa J, Muralha J (2016) The role of tilting rate and wear of surfaces on basic friction angle testing. *ISRM International Symposium - EUROCK 2016*. Vigo, Spain, pp 235–240
- Pérez-Rey I, Alejano LR, González-Pastoriza N et al (2015) Effect of time and wear on the basic friction angle of rock discontinuities. In: *ISRM Regional Symposium, EUROCK 2015*. Salzburg, Austria, pp 1115–1120
- Pérez-Rey I, Alejano LR, Muralha J (2019a) Experimental study of factors controlling tilt-test results performed on saw-cut rock joints. *Geotech Test J* 42:307–330. <https://doi.org/10.1520/GTJ20170375>
- Pérez-Rey I, Alejano LR, Riquelme A, González-deSantos L (2019b) Failure mechanisms and stability analyses of granitic boulders focusing a case study in Galicia (Spain). *Int J Rock Mech Min Sci* 119:58–71. <https://doi.org/10.1016/j.ijrmps.2019.04.009>
- Rabat Á, Cano M, Tomás R (2020a) Effect of water saturation on strength and deformability of building calcarenite stones: correlations with their physical properties. *Constr Build Mater* 232:1–15. <https://doi.org/10.1016/j.conbuildmat.2019.117259>
- Rabat Á, Tomás R, Cano M (2020b) Evaluation of mechanical weakening of calcarenite building stones due to environmental relative humidity using the vapour equilibrium technique. *Eng Geol* 278:1–19. <https://doi.org/10.1016/j.enggeo.2020.105849>
- Rabat Á, Tomás R, Cano M (2021) Advances in the understanding of the role of degree of saturation and water distribution in mechanical behaviour of calcarenites using magnetic resonance imaging technique. *Constr Build Mater* 303:1–24. <https://doi.org/10.1016/j.conbuildmat.2021.124420>

- Rabat Á, Tomás R, Cano M, Miranda T (2020c) Impact of water on peak and residual shear strength parameters and triaxial deformability of high-porosity building calcarenite stones: interconnection with their physical and petrological characteristics. *Constr Build Mater* 262:1–20. <https://doi.org/10.1016/j.conbuildmat.2020.120789>
- Ramana YV, Gogte BS (1989) Dependence of coefficient of sliding friction in rocks on lithology and mineral characteristics. *Eng Geol* 26:271–279. [https://doi.org/10.1016/0013-7952\(89\)90014-8](https://doi.org/10.1016/0013-7952(89)90014-8)
- Ren J, Wang F, He H, Senetakis K (2022) The tribological behavior of analog mudrock interfaces in dry, water-immersed and guar-gum solution states. *Tribol Int* 165:107281. <https://doi.org/10.1016/j.triboint.2021.107281>
- Richards LR (1975) The shear strength of joints in weathered rock. University of London
- Ruiz J, Li C (2014) Measurement of the basic friction angle of rock by three different tilt test methods. In: Alejano LR, Peruchó Á, Olalla C, Jiménez R (eds) *Rock Engineering and Rock Mechanics: Structures in and on Rock Masses - Proceedings of EUROCK 2014*, ISRM European Regional Symposium. CRC Press, Vigo, Spain, pp 261–266
- Singh HK, Basu A (2018) Evaluation of existing criteria in estimating shear strength of natural rock discontinuities. *Eng Geol* 232:171–181. <https://doi.org/10.1016/j.enggeo.2017.11.023>
- Stimpson B (1981) A suggested technique for determining the basic friction angle of rock surfaces using core. *Int J Rock Mech Min Sci Geomech Abstr* 18:63–65. [https://doi.org/10.1016/0148-9062\(81\)90266-7](https://doi.org/10.1016/0148-9062(81)90266-7)
- Tembe S, Lockner DA, Wong TF (2010) Effect of clay content and mineralogy on frictional sliding behavior of simulated gouges: binary and ternary mixtures of quartz, illite, and montmorillonite. *J Geophys Res Solid Earth* 115:1–22. <https://doi.org/10.1029/2009JB006383>
- Tomás R, Cano M, Tomás-Navarro R (2021) Máquina automatizada y reforzada de ensayo de inclinación Tilt Test
- Ulusay R, Karakul H (2016) Assessment of basic friction angles of various rock types from Turkey under dry, wet and submerged conditions and some considerations on tilt testing. *Bull Eng Geol Environ* 75:1683–1699. <https://doi.org/10.1007/s10064-015-0828-4>
- Westbrook JH, Jorgensen PJ (1968) Effects of water desorption on indentation microhardness anisotropy in minerals. *Am Mineral* 53:1899–1909
- Wines DR, Lilly PA (2003) Estimates of rock joint shear strength in part of the Fimiston open pit operation in Western Australia. *Int J Rock Mech Min Sci* 40:929–937. [https://doi.org/10.1016/S1365-1609\(03\)00020-0](https://doi.org/10.1016/S1365-1609(03)00020-0)
- Wyllie DC, Mah CW (2004) *Rock slope engineering: civil and mining*, 4th edn. CRC Press
- Zandarin MT, Alonso E, Olivella S (2013) A constitutive law for rock joints considering the effects of suction and roughness on strength parameters. *Int J Rock Mech Min Sci* 60:333–344. <https://doi.org/10.1016/j.ijrmms.2012.12.007>
- Zhang N, Li CC, Lu A et al (2018) Experimental studies on the basic friction angle of planar rock surfaces by tilt test. *J Test Eval* 47:256–283. <https://doi.org/10.1520/JTE20170308>